



# Quantifying Lithogenic Inputs to the Southern Ocean Using Long-Lived Thorium Isotopes

Habacuc Pérez-Tribouillier<sup>1,2\*</sup>, Taryn L. Noble<sup>1</sup>, Ashley T. Townsend<sup>3</sup>, Andrew R. Bowie<sup>1,2</sup> and Zanna Chase<sup>1</sup>

<sup>1</sup> Institute for Marine and Antarctic Studies, University of Tasmania, Hobart, TAS, Australia, <sup>2</sup> Antarctic Climate and Ecosystems Cooperative Research Centre, Hobart, TAS, Australia, <sup>3</sup> Central Science Laboratory, University of Tasmania, Hobart, TAS, Australia

## OPEN ACCESS

### Edited by:

Benoit Thibodeau,  
The University of Hong Kong,  
Hong Kong

### Reviewed by:

Martin Frank,  
GEOMAR Helmholtz Center for Ocean  
Research Kiel, Germany  
Frank Pavia,  
California Institute of Technology,  
United States

### \*Correspondence:

Habacuc Pérez-Tribouillier  
Habacuc.pereztribouillier@utas.edu.au

### Specialty section:

This article was submitted to  
Marine Biogeochemistry,  
a section of the journal  
Frontiers in Marine Science

**Received:** 28 November 2019

**Accepted:** 16 March 2020

**Published:** 22 April 2020

### Citation:

Pérez-Tribouillier H, Noble TL,  
Townsend AT, Bowie AR and Chase Z  
(2020) Quantifying Lithogenic Inputs  
to the Southern Ocean Using  
Long-Lived Thorium Isotopes.  
*Front. Mar. Sci.* 7:207.  
doi: 10.3389/fmars.2020.00207

Thorium (Th) isotopes were applied to quantify the supply of lithogenic inputs from the Kerguelen Plateau to the Southern Ocean. The dissolved concentrations of <sup>232</sup>Th and <sup>230</sup>Th were measured following a novel pre-concentration method using the Nobias resin from 10 stations above and on the slopes of the plateau. Elevated <sup>232</sup>Th/<sup>230</sup>Th ratios in the upper 500 m of the water column confirm the input of lithogenic material from islands, glaciers and the resuspension of shelf-deposited sediments. <sup>230</sup>Th concentrations were used to calculate a scavenging residence time for Th, which was then applied to calculate the flux of dissolved <sup>232</sup>Th required to match the observed concentrations of dissolved <sup>232</sup>Th. The <sup>232</sup>Th content of the lithogenic material from the Kerguelen Plateau was used with the solubility of Th reported in the literature, to estimate a lithogenic particle flux of 7 to 810 mg m<sup>-2</sup> day<sup>-1</sup>. This flux is comparable to fluxes obtained using sediment traps (8–777 mg m<sup>-2</sup> day<sup>-1</sup>) in other continental-margin zones of the Southern Ocean. The flux of dissolved iron, generated by the dissolution of particles, was also calculated (4,189–6,800 nmol m<sup>-2</sup> day<sup>-1</sup>) based on the iron/thorium ratio in the material from the Kerguelen Plateau. This is higher than previous estimates (1,342 nmol m<sup>-2</sup> day<sup>-1</sup>), suggesting the dissolution of particles as the missing source of iron, thus closing the iron budget of the region. This study confirms the utility of long-lived Th isotopes to quantify lithogenic inputs from continental margin settings.

**Keywords:** thorium, Southern Ocean, Kerguelen Plateau, lithogenic, natural fertilization, GEOTRACES

## INTRODUCTION

The different isotopes of thorium (Th) provide important information about a variety of processes that occur in the oceans. In seawater, Th has a stable oxidation state of IV, making it highly particle reactive (Santschi et al., 2006). Thorium isotopes also have very well-constrained and limited sources to the marine environment. The very-long lived primordial isotope <sup>232</sup>Th ( $t_{1/2} = 1.4 \times 10^{10}$  years) represents ~99.98% of all natural Th and it is supplied to the ocean almost exclusively by the dissolution of continental material transported by rivers, wind and the dissolution of continental shelf sediments (Krishnaswami and Cochran, 2011). <sup>230</sup>Th ( $t_{1/2} = 75,400$  years) is supplied to the ocean almost entirely by the decay of the highly soluble <sup>234</sup>U, which has a uniform distribution in the ocean (Krishnaswami and Cochran, 2008). <sup>230</sup>Th is removed at

an almost constant rate to the sediments by interaction with particles (Anderson et al., 1983). The combination of particle reactivity and well-constrained sources makes Th isotopes one of the most versatile tools to study particle fluxes in the ocean and in the sedimentary record (Francois et al., 1990, 2004; Costa and McManus, 2017; Luo, 2017). In the last decade, the  $^{232}\text{Th}$ - $^{230}\text{Th}$  system has gained popularity as a tracer to quantify lithogenic sources of trace elements to the marine environment (Hsieh et al., 2011; Hayes et al., 2013, 2015, 2017; Deng et al., 2014). The long-lived Th isotopes can be used to track and quantify the input of lithogenic material to the ocean because  $^{232}\text{Th}$  acts as the tracer of lithogenic input, while  $^{230}\text{Th}$  provides information concerning residence time with respect to scavenging, which is assessed through its disequilibrium from its soluble parent nuclide  $^{234}\text{U}$  (Broecker et al., 1973). Finally, with knowledge about the composition and solubility of the lithogenic material it is possible to estimate the input and flux of lithogenic particles and trace elements to the ocean (Hsieh et al., 2011; Hayes et al., 2018).

Trace elements are important because they can limit primary production by phytoplankton in the photic layers of large parts of ocean. In particular, the absence of bio-available iron (Fe) has been recognized to be the main cause of low productivity in areas of the ocean's surface with abundant macronutrients such as nitrogen and phosphorus (known as high nutrient, low chlorophyll or HNLC regions; Martin, 1990; Boyd et al., 2007; Moore et al., 2013). The HNLC regions occupy around one third of the world's oceans, with the Southern Ocean (SO) being the largest of these regions. HNLC conditions are often relieved through the addition of Fe (Morris and Charette, 2013). Outside the SO, Fe is supplied mainly through the dissolution of continental dust transported to the oceans by the wind (Jickells, 2005). However, the SO is located far away from dust sources. Remote islands and shallow continental shelves in the SO can be a natural source of Fe enabling the proliferation of phytoplanktonic blooms (Blain et al., 2001; Tyrrell et al., 2005; Tagliabue et al., 2009, 2014), and hence influencing the oceanic carbon cycle and the sequestration of  $\text{CO}_2$  from the atmosphere (Fung et al., 2000; Sarthou et al., 2007; Mahowald et al., 2009; Boyd and Ellwood, 2010).

The Kerguelen Plateau (KP) area hosts the largest phytoplankton bloom of the SO (Blain et al., 2007). It appears in the austral summer after photosynthesis is no longer light-limited, and extends over more than 45,000  $\text{km}^2$ . A series of voyages carried out during 2005 and 2011 (KEOPS1 and 2) significantly increased the understanding of how natural Fe fertilization occurs and its important role in the global carbon cycle, and noted the importance of islands in the supply of iron to Antarctic and Subantarctic regions (Blain et al., 2007, 2008a,b; Jacquet et al., 2008; Jouandet et al., 2008; Mosseri et al., 2008; Sarthou et al., 2008). Remote-sensing and modeling were able to simulate bloom conditions over the plateau and contributed to constrain the processes that transport iron, acknowledging the importance of the bathymetry and surface advection fields (Bopp et al., 2008; Mongin et al., 2008), which was further confirmed by detailed descriptions of the region's physical oceanography and its relation with the flow of the Antarctic Circumpolar Current

(ACC; **Figure 1**; Park et al., 2008a,b, 2014). Particle dynamics (Venchiarutti et al., 2008, 2011) and carbon fluxes (Savoye et al., 2008; Planchon et al., 2015) were studied through the analysis of Th isotopes in the dissolved and particulate phases of seawater. Other work focused on constraining the origin of the lithogenic material that allows Fe to sustain the phytoplankton bloom (van Beek et al., 2008; Zhang et al., 2008; van der Merwe et al., 2015; Grenier et al., 2018). The dominant source of iron was found to be the dissolution of sediments deposited on the plateau and transported to the surface by vertical mixing (Zhou et al., 2014), and the lateral transport and dissolution of lithogenic material supplied by the Kerguelen Islands (van Beek et al., 2008; Sanial et al., 2015; van der Merwe et al., 2015). It was found that the bloom persisted even with Fe concentrations close to values known to be metabolically limiting for phytoplankton (Bowie et al., 2015). This highlights the importance of efficient Fe recycling in the mixed layer, as well as of other potential sources of Fe to the region, e.g., from Heard and McDonald Islands (HIMI) in the central part of the plateau (Bown et al., 2012; Bowie et al., 2015).

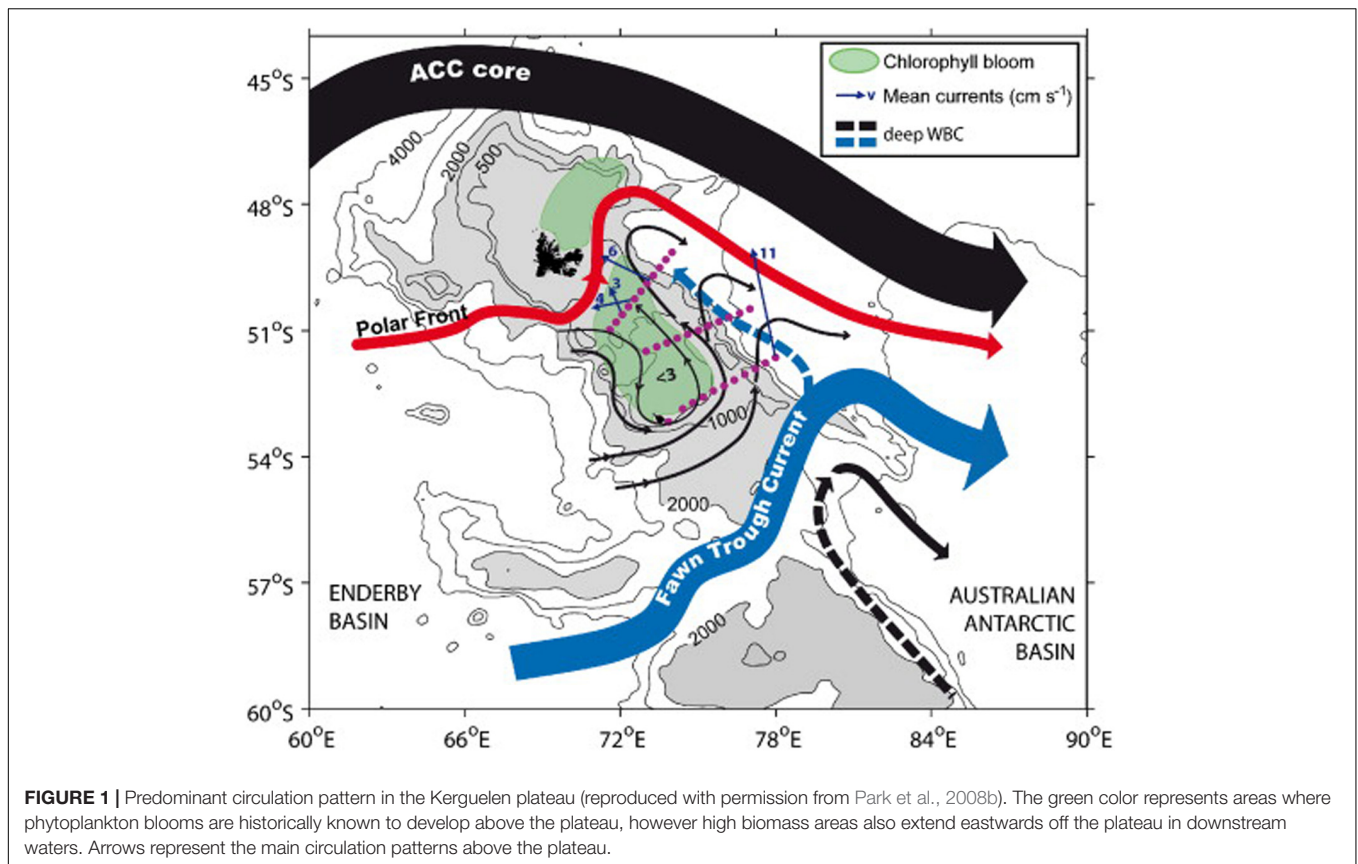
The Heard and McDonald Earth-Ocean-Biosphere Interactions study (HEOBI; GEOTRACES process study G1pr05), undertaken during the summer of 2016, focused on sampling the central part of the KP around HIMI. The main objectives of this voyage were to increase knowledge about the contribution of HIMI and surrounding shallow areas to the biogeochemical cycle of Fe in the region. Special attention was paid to the role of particles originating from the islands as well as any possible hydrothermal contribution to the Fe inventory. Results from this expedition noted the importance of HIMI to Fe availability that influences the drawdown of nutrients above the plateau (Holmes et al., 2019), and also confirmed that glacial erosion from Heard Island and probably hydrothermal activity from McDonald Island can support the previously unaccounted biological demand (van der Merwe et al., 2019). The aim of this work was to apply dissolved  $^{232}\text{Th}$  and  $^{230}\text{Th}$  measurements in samples collected during the HEOBI voyage in order to quantify the input of lithogenic material released from the areas around HIMI. This lithogenic material has the potential to release iron and therefore, to naturally fertilize surface waters around and in the wake of the KP.

## MATERIALS AND METHODS

### Sampling

Seawater samples and hydrographic data<sup>1</sup> were collected in the KP region during the HEOBI voyage in January and February 2016 onboard the R/V Investigator (IN2016\_V01; **Figure 2**). All sampling was performed following the protocols described in the GEOTRACES intercalibration for Th and Pa isotopes (Anderson et al., 2012). Samples ranging from 5 to 10 L were collected directly from Niskin bottles mounted on a standard CTD and filtered through AcroPak capsule filters (0.2  $\mu\text{m}$ ) into

<sup>1</sup><http://www.marlin.csiro.au/geonetwork/srv/eng/search#16ba5a0ce-b87a-4bda-b16c-3527279c3bca>



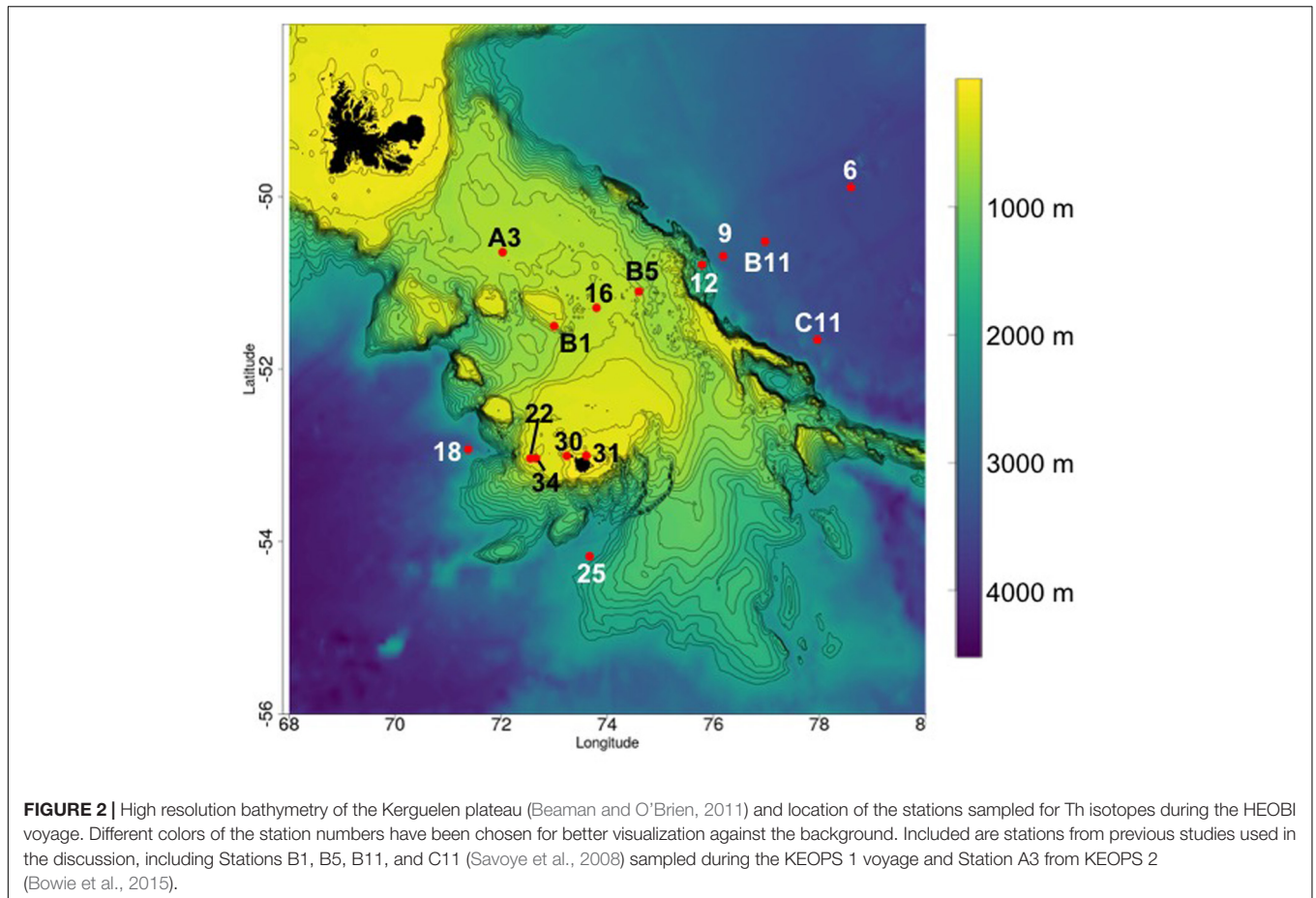
10 L pre-weighed plastic containers. Samples were then acidified with 1 mL of 11M HCl distilled acid per liter of sample to a final pH value  $\sim 1.7$ . In order to determine procedural blank concentrations, 2 L of ultra-high purity water (UPW) were collected from the onboard system and acidified in the same way as the samples. In total, 75 samples from 10 different locations (Figure 2) were pre-concentrated and analyzed. Two stations (18 and 25) were sampled on the western flank of the plateau in waters located generally upstream of the plateau; the water column characteristics at sampling time support their use as reference stations. A series of samples was collected within 1 km of Heard (30 and 31) and McDonald (22 and 34) Islands in order to establish a Th signal from the islands. Station 16 was collected from the middle of the plateau and is part of a transect that includes stations 6, 9, and 12 that were collected to sample the transition from the plateau ( $\sim 450$  m depth) to open water (3600 m depth) sub-Antarctic conditions.

## Pre-concentration and Column Chemistry

The pre-concentration and chromatographic separation methodology applied in this study was part of a technique to simultaneously determine Th and neodymium (Nd) isotopes from a single seawater sample, and is described in full detail in Pérez-Tribouillier et al. (2019). Briefly, samples were amended with  $\sim 200$   $\mu\text{L}$  of concentrated hydrofluoric acid (HF) and spiked with 1 pg of  $^{229}\text{Th}$  per kg of seawater. Samples were left

to equilibrate for at least 48 h. After this period, enough 2.5M ammonium acetate buffer solution was added to reach a final concentration in the sample of 0.05M. The pH was then adjusted to 4.75 with concentrated HCl. Immediately thereafter, samples were pumped through an array of two Nobias PA1L cartridges. Once all sample passed through the cartridges, remaining salts were washed off the resin with UPW. Finally, Th and other trace elements were eluted with 5 mL of 3M  $\text{HNO}_3$ .

After pre-concentration, samples were oxidized with 0.5 mL of a mixture of concentrated  $\text{HNO}_3$  and  $\text{HClO}_4$  (4:1) at  $200^\circ\text{C}$  in order to remove any organic substances (originating from either the sample, or from the column extraction). Thorium isotopes were chromatographically separated and purified using 1 mL Bio-Rad AG1-X8 anion exchange resin following protocols described in Anderson et al. (2012). Samples were transformed to the HCl form and loaded onto the pre-conditioned resin in order to remove transition metals as well as uranium and protactinium isotopes. The samples were oxidized again and converted into 8M  $\text{HNO}_3$  form and loaded onto the same resin (pre-conditioned with 8M  $\text{HNO}_3$ ) to remove the rare earth elements. Thorium isotopes were finally eluted from the resin with 11M HCl, oxidized and redissolved in 0.6 mL 2%  $\text{HNO}_3$  + 0.3% HF in preparation for analysis. Sample processing occurred in batches consisting of six samples. For each different CTD station, a 2.5 L UPW procedure blank (spiked with  $^{229}\text{Th}$ ) and the intercalibrated reference material SW2010-2 (Anderson et al., 2012) were processed. An aliquot of  $\sim 0.5$  g of



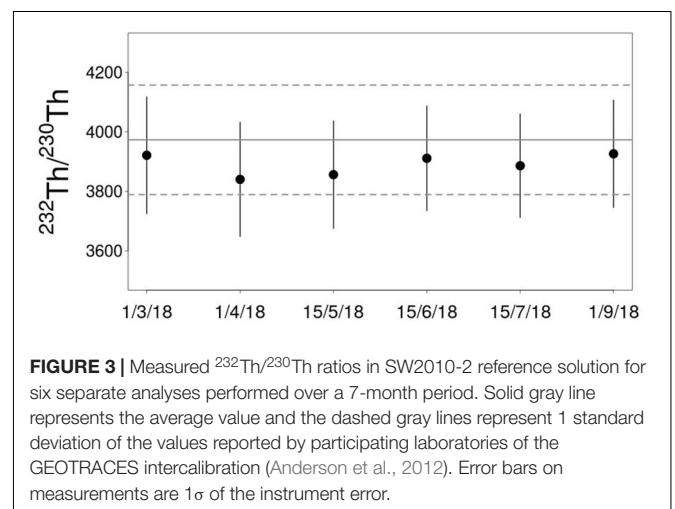
this reference material was diluted in 2.5 L of UPW. Both the blank and the reference material were treated in the same way as the samples, including pre-concentration and column chemistry. The measurement of Th isotopes was performed on an Element 2 SF-ICP-MS at the Central Science Laboratory (University of Tasmania), with sample introduction via an Aridius II Desolvating Nebulizer to minimize oxide/hydrate formation. The pre-concentration factor of the solution introduced to the instrument is about 16,000 for a 10 L sample.

### Blanks and Quality Control

In order to reduce blank contributions, all sample processing was performed inside a ducted laminar-flow hood (ISO-1 conditions) in an ISO-5 environment. The procedural blank values ranged from 2–17 pg and 0.2–1.8 fg for  $^{232}\text{Th}$  and  $^{230}\text{Th}$ , respectively. The reproducibility of the intercalibrated reference material SW2010-2 remained within 5% of the reported values over a period of 7 months (Figure 3), indicating good method reliability.

### Data Treatment

$^{232}\text{Th}$  and  $^{230}\text{Th}$  signals were corrected for instrument blank and measurement mass bias (Pérez-Tribouillier et al., 2019). Thereafter,  $^{232}\text{Th}$  and  $^{230}\text{Th}$  concentrations were obtained using isotope dilution equations (Sargent et al., 2002). Finally, an



average procedural blank, based on the blank determinations from all stations, was subtracted. For  $^{230}\text{Th}$ , the procedural blank represented < 5% of the total signal, however it increased toward 10% for shallower samples. For  $^{232}\text{Th}$  the blank contribution was generally less than 3%. The measured  $^{230}\text{Th}$  concentrations were corrected for ingrowth due to decay of  $^{234}\text{U}$  during the



storage period. The initial content of  $^{234}\text{U}$  was calculated based on the  $^{238}\text{U}$  activity of each sample, obtained through the salinity relationship of Owens et al. (2011) and a  $\delta^{234} = 146.8 \pm 0.1\text{‰}$  (Andersen et al., 2010). With this information, the ingrowth-corrected ( $^{230}\text{Th}_{\text{IGC}}$ ) was calculated using the sample  $^{234}\text{U}$  activity, a  $\lambda^{234}$  of  $2.8263 \times 10^{-6} \text{ yr}^{-1}$  and a sample storage time of 2 years (Eq. 1). The ingrowth correction varies from 5 to 50% and is higher toward the surface of each station because of the lower  $^{230}\text{Th}$  concentrations.

$$^{230}\text{Th}_{\text{IGC}} = ^{230}\text{Th} - ^{234}\text{U} \times \left(1 - e^{(\lambda \times \text{years})}\right) \quad (1)$$

The contribution of lithogenic  $^{230}\text{Th}$  was estimated using the measured  $^{232}\text{Th}$  concentration of each sample and a  $^{230}\text{Th}/^{232}\text{Th}$  for the lithogenic material of  $4.0 \times 10^{-6} \text{ mol/mol}$  (Roy-Barman et al., 2009). The lithogenic contribution was subtracted from the total dissolved  $^{230}\text{Th}$  to obtain the excess  $^{230}\text{Th}$  ( $^{230}\text{Th}_{\text{xs}}$ ; Eq. 2). The contribution of lithogenic  $^{230}\text{Th}$  is less than 2% for most samples considered.

$$^{230}\text{Th}_{\text{xs}} = ^{230}\text{Th}_{\text{IGC}} - ^{232}\text{Th}_{\text{measured}} \times \left[^{230}\text{Th}/^{232}\text{Th}\right]_{\text{litho}} \quad (2)$$

A  $^{230}\text{Th}$  residence time ( $230\text{RT}$ ) was calculated for each station as shown in Eq. 3 (Hayes et al., 2013). Additionally, Eq. 4 was used to calculate a  $^{234}\text{Th}$  residence time ( $234\text{RT}$ ).

$$230\text{RT}(z) = \frac{\int_0^z \text{dissolved } ^{230}\text{Th}_{\text{xs}} \text{ activity } dz}{\int_0^z ^{234}\text{U activity} \times \lambda_{230} dz} \quad (3)$$

$$234\text{RT}(z) = \frac{\int_0^z ^{234}\text{Th activity}/^{238}\text{U activity } dz}{1 - \int_0^z ^{234}\text{Th activity}/^{238}\text{U activity } dz} \times \tau_{234} \quad (4)$$

The dissolved  $^{230}\text{Th}_{\text{xs}}$  activity was defined as the measured concentration converted into activity units (dpm), the  $^{234}\text{U}$  activity was obtained from the measured salinity, and  $\lambda_{230}$  ( $9.2 \times 10^{-6} \text{ year}^{-1}$ ) as the radioactive decay rate of  $^{230}\text{Th}$  where  $z$  is the depth of integration. For the  $234\text{RT}$ , dissolved  $^{234}\text{Th}$  and  $^{238}\text{U}$  activities reported in Savoye et al. (2008) for the KEOPS 1 voyage were used and  $\tau_{234}$  is the mean life of  $^{234}\text{Th}$  ( $1/\lambda$ ). The  $230\text{RT}$  was then used to calculate a dissolved  $^{232}\text{Th}$  flux by dividing the depth-integrated  $^{232}\text{Th}$  inventory by the residence time (Eq. 5; Hayes et al., 2013):

$$\text{Dissolved } ^{232}\text{Th flux}(z) = \frac{\int_0^z \text{dissolved } ^{232}\text{Th } dz}{\tau_{\text{Th}}(dz)} \quad (5)$$

The dissolved  $^{232}\text{Th}$  flux was then used to estimate a particulate lithogenic flux considering the content of  $^{232}\text{Th}$  in the basaltic lithogenic material around the KP (5.3 ppm; Duncan et al., 2016) and the fractional solubility of  $^{232}\text{Th}$  in lithogenic material ( $S_{\text{Th}}$ ; Arraes-Mescoff et al., 2001; Roy-Barman et al., 2002) as shown in Eq. 5 (Hayes et al., 2013).

$$\text{Lithogenic flux}(z) = \frac{\text{Dissolved } ^{232}\text{Th flux}(z)}{[\text{Th}]_{\text{Kerg}} \times S_{\text{Th}}} \quad (6)$$

Subsequently with knowledge about the composition and solubility of metals relative to  $^{232}\text{Th}$ , it is possible to produce an estimation of dissolved metal fluxes originating from the dissolution of lithogenic particles as follows (Hayes et al., 2013):

$$\text{Dissolved metal flux} = \left[ \frac{\text{metal}}{^{232}\text{Th}} \right]_{\text{Kerg}} \times \left( \frac{S_{\text{metal}}}{S_{\text{Th}}} \right) \times \text{Dissolved } ^{232}\text{Th flux} \quad (7)$$

## RESULTS

### Water Mass Distribution During the HEOBI Voyage

The temperature-salinity diagram (Figure 4) indicates that the samples from stations located near HIMI (stations 22,30,31,34), all from depths < 200 m, have salinities (absolute salinity units) below  $34.1 \text{ g kg}^{-1}$  and temperature above  $2^\circ\text{C}$ , consistent with properties of the Antarctic Surface Water (AASW). The same is the case for surface samples (<200 m) from other stations, with the exception of Station 6. At Station 6, above 75 m the water temperature was greater than  $4.5^\circ\text{C}$  and density below 26.75. These characteristics might indicate transient seasonal warming of the upper water column. Below the mixed layer, at depths between 150 and 300 m, Stations 9, 16, 18, and 25 exhibited a subsurface temperature minimum ( $<2^\circ\text{C}$ ) and fresher water ( $<34.2 \text{ g kg}^{-1}$ ) than deeper layers. These characteristics match the definition of Winter Water reported for the KP, centered at  $\sim 200 \text{ m}$  water depth (Park et al., 2008b). Below 300 m there is a transition to Upper Circumpolar Deep Water (UCDW) associated with a temperature maximum of  $\sim 2.5^\circ\text{C}$  and an oxygen minimum ( $180 \text{ } \mu\text{mol L}^{-1}$ ). A deep salinity maximum confirms the presence of Lower Circumpolar Deep Water (LCDW). Below 2,600 m, Stations 6, 9, and 18 display properties consistent with the presence of Antarctic Bottom Water (AABW), i.e., low temperature and salinity but with a higher oxygen content towards the bottom (Park et al., 2008b). This water-column composition is typical for the austral summer (Park et al., 1998) and is consistent with the findings of other studies (Park et al., 2008b, 2014; Park and Vivier, 2011; Holmes et al., 2019).

### $^{232}\text{Th}$ and $^{230}\text{Th}$ Concentrations Plateau and Off-Plateau Stations

All  $^{230}\text{Th}$  and  $^{232}\text{Th}$  concentration data can be found in Supplementary Table 1.  $^{230}\text{Th}_{\text{xs}}$  concentrations in the samples range from  $0.7 \text{ fg kg}^{-1}$  (Station 18, 60 m) to  $18.2 \text{ fg kg}^{-1}$  (CTD6, 3579 m). These values are similar to other parts of the SO including the Weddell Sea (Rutgers van der Loeff and Berger, 1993), the Drake Passage (Venchiarutti et al., 2011), the Crozet Basin (Coppola et al., 2006) and particularly similar to a previous study in the KP (Venchiarutti et al., 2008).

All profiles indicate a somehow linear increase of  $^{230}\text{Th}_{\text{xs}}$  concentration with depth (Figure 5). The “slope” of this increase seems to be different in the top 600 m of the

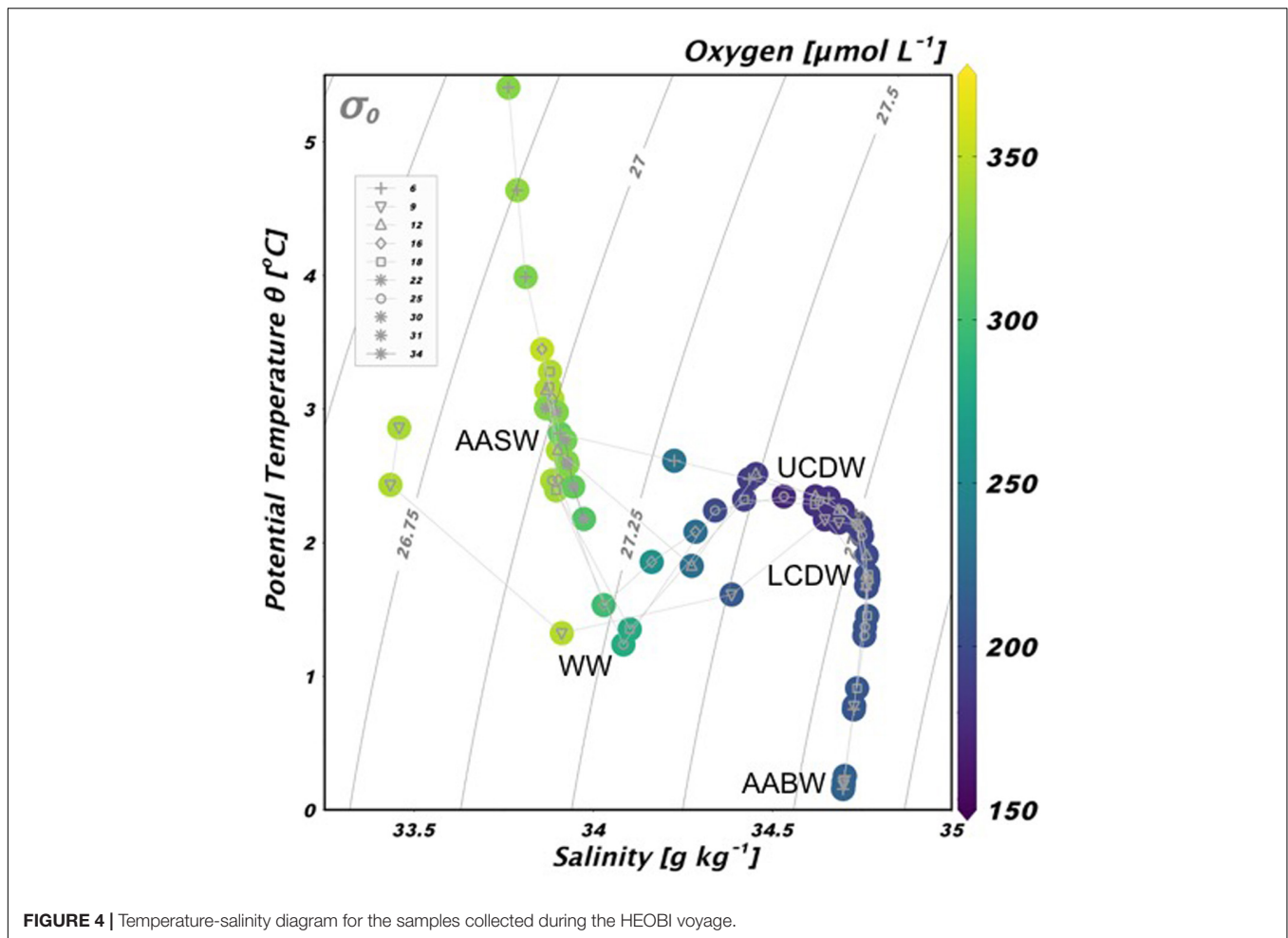


**FIGURE 4** | Temperature-salinity diagram for the samples collected during the HEOBI voyage.

water column, compared to the water column below this depth. Additionally, Stations 16 and 18 show a depletion of  $^{230}\text{Th}_{\text{xs}}$  toward the bottom. Similar mixed features in  $^{230}\text{Th}_{\text{xs}}$  concentration profiles have been observed in other oceanic settings in the Southern Atlantic (Moran et al., 2002; Deng et al., 2014), the Arctic (Trimble et al., 2004), and along the path of the ACC (Rutgers van der Loeff and Berger, 1993; Venchiarutti et al., 2011), including the KP (Venchiarutti et al., 2008).

The dissolved  $^{232}\text{Th}$  concentrations range from 6.9  $\text{pg kg}^{-1}$  (CTD12, 30 m) to 101  $\text{pg kg}^{-1}$  (CTD25, 200 m). Most of our data is within the same order of magnitude of previous  $^{232}\text{Th}$  concentrations reported on the plateau by Venchiarutti et al. (2008). However, these authors report several samples with higher concentration that in some cases are as much as 4.5 times greater (450  $\text{pg kg}^{-1}$ ) than the maximum values found in our study.

With the exception of Stations 18 and 12, all profiles show a spike in the  $^{232}\text{Th}$  concentration in the top 600 m of the water column. Below that depth,  $^{232}\text{Th}$  concentrations generally increase with depth, however some spikes stand out in all the stations (excepting Station 18; **Figure 5**).

In particular, Station 25 shows two prominent peaks at 200 m (100  $\text{pg kg}^{-1}$ ) and 1200 m (87  $\text{pg kg}^{-1}$ ). Such concentrations could very easily be a result of contamination during sampling or analysis. However, the blank contribution at that station remained low. Therefore, and because of the higher concentrations previously reported for the plateau (Venchiarutti et al., 2008), we prefer not to exclude those measurements.

### Near-Island Shallow Stations

The  $^{232}\text{Th}$  and  $^{230}\text{Th}$  concentrations in samples collected close to Heard (Stations 30, 31) and McDonald (Stations 22, 34) Islands (**Figure 2**) are similar regardless of location or depth [average of  $87.5 \pm 13 \text{ pg kg}^{-1}$  (1- $\sigma$ ); **Table 1**]. These concentrations are amongst the highest of our data set and can be compared with  $^{232}\text{Th}$  concentrations found near Heard Island during the KEOPS 1 expedition (84–273  $\text{pg kg}^{-1}$ ; Venchiarutti et al., 2008).  $^{230}\text{Th}_{\text{xs}}$  concentrations average  $2.7 \pm 1.2 \text{ fg kg}^{-1}$  (1- $\sigma$ ) (**Table 1**). These concentrations are higher than those reported in the previously mentioned study around HIMI (0.5–1.35  $\text{fg kg}^{-1}$ ). In particular, the  $^{230}\text{Th}$  concentration of Station 30 at 75 m (5.4  $\text{fg kg}^{-1}$ ) is unusually high for that depth

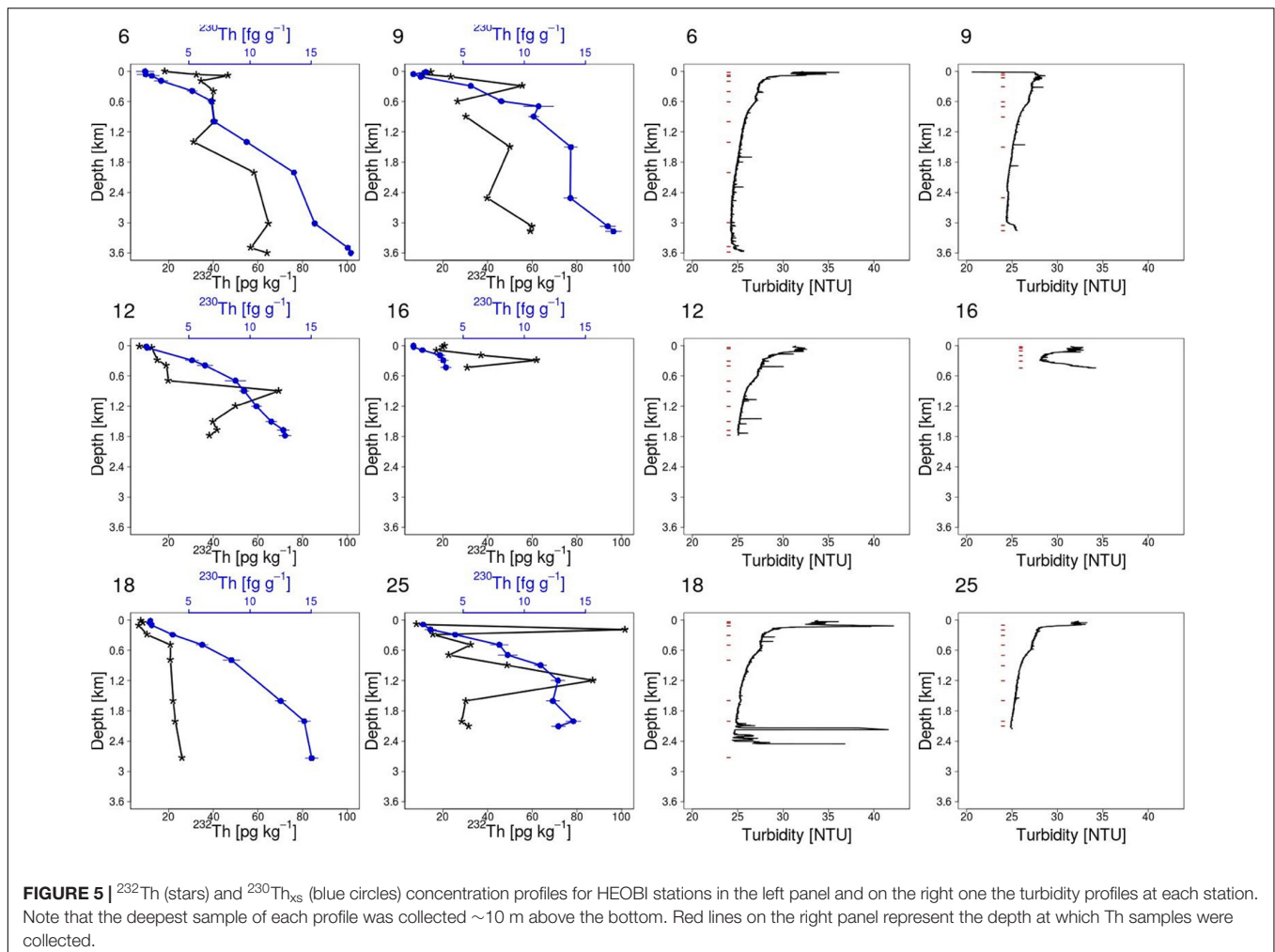


**FIGURE 5** |  $^{232}\text{Th}$  (stars) and  $^{230}\text{Th}_{\text{xs}}$  (blue circles) concentration profiles for HEOBI stations in the left panel and on the right one the turbidity profiles at each station. Note that the deepest sample of each profile was collected  $\sim 10$  m above the bottom. Red lines on the right panel represent the depth at which Th samples were collected.

compared to previous studies in the region (Coppola et al., 2006; Venchiarutti et al., 2008).

### $^{232}\text{Th}/^{230}\text{Th}$ Ratios

The highest  $^{232}\text{Th}/^{230}\text{Th}$  ratios were found near HIMI (Table 1 and Figure 6), with a maximum value of 32,600 found in Station 34 at the boundary between the WW and the AASW ( $\sigma_\theta = 27.15$ ; 122 m depth), and the lowest value of 1,735 in the LCDW component of reference Station 18 ( $\sigma_\theta = 27.8$ ; 2,200 m depth).

All stations show an increase of the  $^{232}\text{Th}/^{230}\text{Th}$  ratio above the UCDW ( $\sigma_\theta < 27.5$ ; 600 m), except Station 18, which exhibits an almost uniform ratio with depth (Figure 6). In the UCDW and below, Stations 6 and 9 also display a uniform  $^{232}\text{Th}/^{230}\text{Th}$  ratio. Additionally, stations 12 and 25 exhibit  $^{232}\text{Th}$  enrichments at 900 ( $\sigma_\theta = 27.7$ ) and 1,200 m ( $\sigma_\theta = 27.8$ ), respectively. The samples collected around McDonald Island present a higher  $^{232}\text{Th}/^{230}\text{Th}$  (24,821–32,600) ratio compared to the samples collected around Heard Island (12,870–16,938).

**TABLE 1** |  $^{232}\text{Th}$ ,  $^{230}\text{Th}_{\text{xs}}$ , and  $^{232}\text{Th}/^{230}\text{Th}$  ratio in the near-island stations 22, 30, 31, and 34.

Station	Depth [m]	$^{232}\text{Th}$ [ $\mu\text{g kg}^{-1}$ ]	$1-\sigma$ [ $\mu\text{g kg}^{-1}$ ]	$^{230}\text{Th}_{\text{xs}}$ [ $\text{fg kg}^{-1}$ ]	$1-\sigma$ [ $\text{fg kg}^{-1}$ ]	$^{232}\text{Th}/^{230}\text{Th}$
34	50	97	1.9	2.8	0.3	$28,695 \pm 1545$
34	80	94.3	1.9	4.1	0.4	$25,278 \pm 1361$
34	122	81.5	1.6	3.9	0.2	$32,600 \pm 1756$
31	45	81.3	1.6	3.5	0.2	$16,938 \pm 912$
30	88	59.8	1.2	2.5	0.2	$16,162 \pm 918$
30	75	88.8	1.8	5.5	0.4	$12,870 \pm 731$
22	151	100.8	2.0	2.3	0.2	$27,243 \pm 1853$
22	190	96.8	1.9	2.5	0.2	$24,821 \pm 1688$

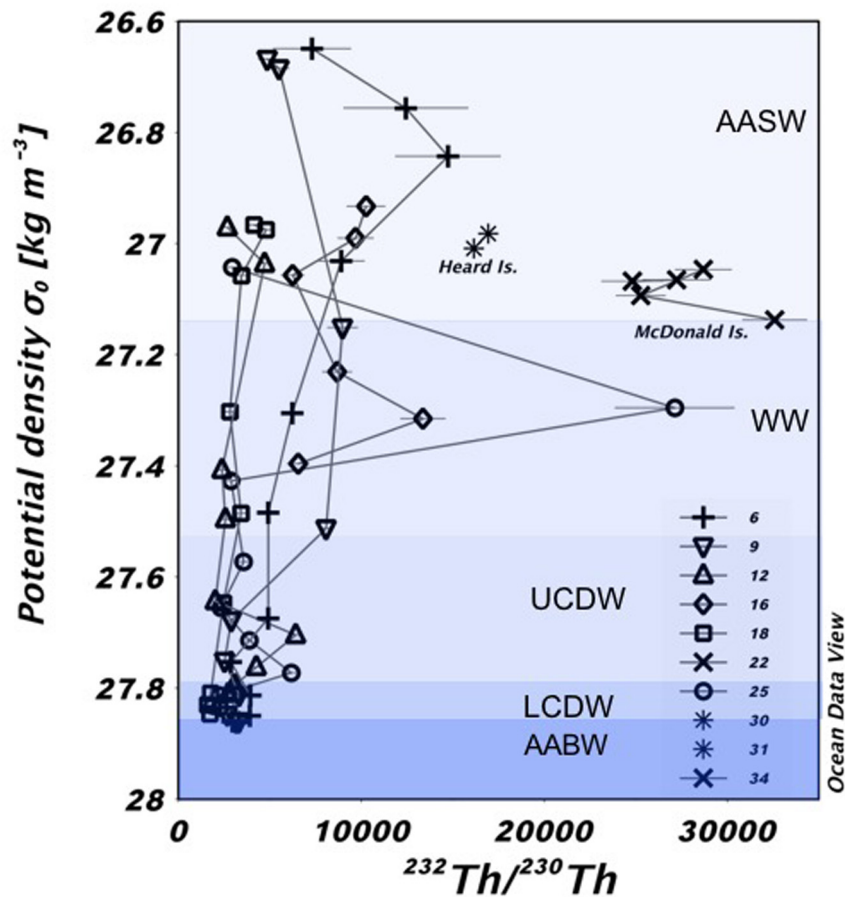


**FIGURE 6** |  $^{232}\text{Th}/^{230}\text{Th}$  ratio plotted against potential density anomaly for the HEOBI samples. Different background shading indicates the different water masses present during the HEOBI sampling campaign. The analytical standard error of many of the samples are smaller than the symbol. Note that the bottom sample of each station was collected  $\sim 10$  m above the seafloor.

## DISCUSSION

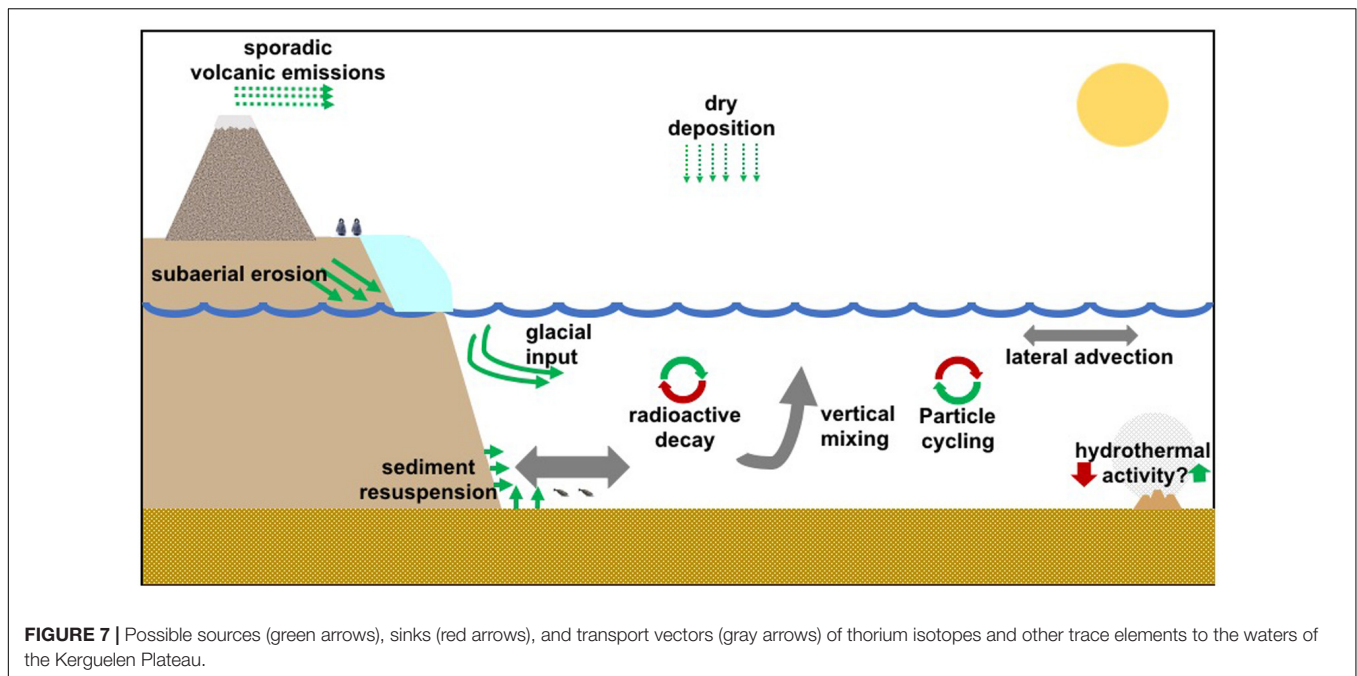
### $^{232}\text{Th}$ Enrichments Above the Plateau and the Role of Circulation

Lithogenic material from the plateau allows the development of productivity once the light is no longer limiting in the region. Supplied by the direct subaerial erosion of the islands, glacial input (subglacial and fluvial discharge) and the resuspension of continental shelf sediments, this material releases  $^{232}\text{Th}$ , Fe and other trace elements (Figure 7). Because  $^{232}\text{Th}$  is only supplied to the ocean by the dissolution of lithogenic material, an increase in the  $^{232}\text{Th}$  concentration can be indicative of the supply from the Kerguelen Plateau. The spikes in the  $^{232}\text{Th}$  concentration near the surface of Stations 6, 9, and 25 can be associated with the direct dissolution of particles, introduced in the surface and transported downward. This is somehow confirmed by the turbidity data (Figure 5, right panel) that indicate the highest particle loads toward the surface. However, in Stations 9, 12 and 25, mid-depth spikes in the  $^{232}\text{Th}$  concentration cannot be explained by the direct dissolution of lithogenic material because there are not

increased turbidity values at those particular depths, therefore this  $^{232}\text{Th}$  must have been laterally advected from other parts of the plateau. Surprisingly, only Stations 16 and 18 present a nepheloid layer. This layer is reflected in a depletion in  $^{230}\text{Th}$  concentration in the deepest samples of those stations due to enhanced scavenging by particles resuspended from the bottom. However, these particles do not seem to be a source of dissolved  $^{232}\text{Th}$ , very likely because of their low reactivity.

The  $^{232}\text{Th}/^{230}\text{Th}$  ratio can therefore be used to track supply of lithogenic material to the ocean because  $^{232}\text{Th}$  is released only by the dissolution of lithogenic material (in a similar way as Fe). Under open-ocean conditions, it might be expected that the  $^{232}\text{Th}/^{230}\text{Th}$  ratio would decrease with increasing depth. Such behavior can be seen at Station 18 (Figure 6, squares) where the  $^{232}\text{Th}/^{230}\text{Th}$  goes from  $4800 \pm 396$  near the surface ( $\sigma_\theta = 27$ ; 65 m) to  $1731 \pm 65$  near the bottom ( $\sigma_\theta = 27.8$ ; 2,725 m). A similar pattern can be seen in Station 6 below 100 m ( $\sigma_\theta = 26.8$ ), where the  $^{232}\text{Th}/^{230}\text{Th}$  ratio is  $14,743 \pm 2876$ , and decreases with depth to  $3,288 \pm 20$  ( $\sigma_\theta = 27.9$ ; 3,576 m). These findings, allow us to establish Station 18 as a reference site of oceanic conditions. In contrast, the rest of the stations





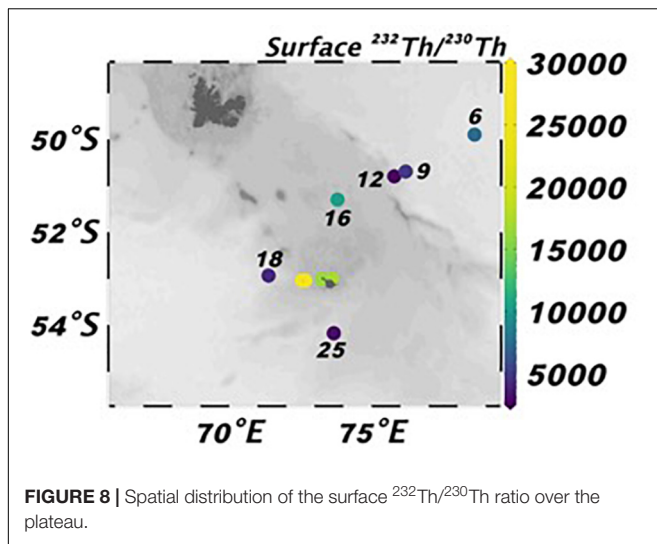
show (to different extents)  $^{232}\text{Th}$  enrichments to the AASW and WW components of the water column ( $\sigma_\theta < 27.5$ ; depth < 300 m). These enrichments are the “fingerprint” of the lithogenic material from the KP. As expected, this imprint is more intense for the stations located near HIMI because they provide a constant input of lithogenic material which supplies  $^{232}\text{Th}$  but not  $^{230}\text{Th}$ , resulting in the highest  $^{232}\text{Th}/^{230}\text{Th}$  ratios. The highest of which are found near Stations 22 (24,821–27,243) and 34 (25,278–32,600), located close to McDonald Island. Near Heard Island, Stations 30 (12,870–16,162) and 31 (16,938), also show elevated  $^{232}\text{Th}/^{230}\text{Th}$  ratios, although not as high as near McDonald Island. This difference can be explained because of the different content of  $^{232}\text{Th}$  in basalts from McDonald ( $28 \pm 19$  ppm) and Heard ( $5 \pm 2$  ppm) islands respectively (J. Fox, personal communication).

Once the lithogenic material supplied by the islands enters the ocean, it releases dissolved  $^{232}\text{Th}$ , Fe and other trace elements. These dissolved elements as well as some lithogenic particles can be transported away from the islands via local circulation enabling a downstream development of productivity. In fact, the historical position of both branches of the bloom that occurs above the KP (Figure 1, green areas) match with the main trajectories of the circulation of the PF and the topography-controlled circulation in the northern and central parts of the plateau.

Considering  $^{232}\text{Th}/^{230}\text{Th}$  as a fingerprint of lithogenic input and that most of the lithogenic material is supplied to surface waters, a gradient in  $^{232}\text{Th}$  enrichment would be expected, being stronger near the source and decreasing as the signal is transported away. Zhang et al. (2008) confirmed, through the use of rare earth elements (REE), the recent dissolution of basaltic material close to the Kerguelen Archipelago (KA) and HIMI, and suggested that this material is transported by the

predominant circulation patterns in the northern and central parts of the KP, respectively (Figure 1). Neodymium isotopic composition ( $\epsilon_{\text{Nd}}$ ) data further proved this transport from the KA to the stations located north of the Polar Front (Grenier et al., 2018), and our own  $\epsilon_{\text{Nd}}$  and REE data also confirms that the material supplied close to HIMI is transported northwards, all the way to the southern edge of the Polar Front (Pérez-Tribouillier et al., unpublished).

Our Th data over the plateau lacks the spatial distribution necessary to accurately track the possible pathways of surface/subsurface circulation. However, some patterns do exist in the  $^{232}\text{Th}/^{230}\text{Th}$  distribution that seem to confirm the importance of the HIMI for the natural fertilization of the waters north and to the east of these islands (Figure 8). Specifically, the near-surface  $^{232}\text{Th}/^{230}\text{Th}$  ratio is highest near HIMI ( $22,259 \pm 6600$ ,  $n = 8$ ). In the middle of the plateau at Station 16 this value decreases to  $10,262 \pm 1042$ . Considering the predominant northwards circulation in this part of the plateau (Figure 1, Park et al., 2008b), this lower  $^{232}\text{Th}/^{230}\text{Th}$  value at Station 16 could very well be attributed to a dilution of the HIMI signal. This hypothesis is supported by the low  $^{232}\text{Th}/^{230}\text{Th}$  ratio ( $4141 \pm 341$ ) at Station 18. This station is located before the circulation turns west toward HIMI and therefore at this point, seawater has not yet received any lithogenic material from the plateau. After the current passes next to HIMI, it travels north toward Station 16 at a speed of  $\sim 2.6 \text{ km day}^{-1}$  (Park et al., 2008b), a component turns east and reaches Station 9 where the value decreases to  $4853 \pm 500$ . The enrichment at Station 12 is even smaller ( $2,683 \pm 240$ ). We hypothesize that this low value is associated with the western boundary current that flows along the eastern flank of the plateau and flushes away  $^{232}\text{Th}$  from Station 12. The surface enrichment at Station 6 ( $7,300 \pm 200$ ) is higher than at station 9, even though Station 6 is further away



from the plateau. In this region however, the circulation from the central KP converges with the flow of the PF, plausibly driving an increase in surface  $^{232}\text{Th}/^{230}\text{Th}$  ratios. More detailed sampling above the central part of the plateau, especially between HIMI and Station 16 would have been useful to better constrain the circulation over the plateau using the  $^{232}\text{Th}/^{230}\text{Th}$  signal.

### Th-Scavenging Removal Residence Time in Surface Waters of the Kerguelen Plateau

The calculation of  $^{232}\text{Th}$  fluxes requires information about its removal rate from the dissolved fraction of seawater. This residence time can be obtained from the less abundant isotopes  $^{228}\text{Th}$ ,  $^{230}\text{Th}$ , and  $^{234}\text{Th}$  and the disequilibria from their parent nuclides, making two assumptions: (1) considering a steady state, and (2) by neglecting physical transport.

The short lived  $^{234}\text{Th}$  isotope ( $t_{1/2} = 24.1$  days) is routinely used to estimate the export of particulate organic carbon from the surface of the ocean (Buesseler et al., 1992; Cochran et al., 2000).  $^{230}\text{Th}$  has also been used to calculate surface residence times (Luo et al., 1995; Hsieh et al., 2011; Hayes et al., 2013; Deng et al., 2014; Lopez et al., 2015). However, differences have been found in the surface scavenging residence times obtained through the use of both isotopes. In the Equatorial Pacific, Luo et al. (1995) found significantly higher  $^{230}\text{Th}$  residence times ( $RT_{230}$ ) in the euphotic zone, compared to the ones obtained with  $^{234}\text{Th}$  and  $^{228}\text{Th}$  data. This was attributed to the longer half-life of  $^{230}\text{Th}$ , which allows for “pre-formed”  $^{230}\text{Th}$  to be transported from deeper waters to the surface through water mixing processes, thereby violating one of the basic assumptions of this method, and producing an over-estimation of its scavenging residence time. Hayes et al. (2013) also emphasize the possible impact of vertical mixing to surface scavenging residence times calculated with  $^{230}\text{Th}$  data in the Pacific, however, these authors did not have  $^{234}\text{Th}$  data available for comparison. In the tropical and subtropical regions of the Atlantic Ocean,  $^{234}\text{Th}$  and  $^{230}\text{Th}$  residence time estimates for the top 25 m of

the water column seem to be in more agreement (Hsieh et al., 2011). However, some discrepancies remain in the equator and higher latitudes, that again, could be very well-explained by the upwelling of  $^{230}\text{Th}$ .

In several sectors of the Southern Ocean, including the Kerguelen Plateau, the assumption of no vertical transport could be severely violated, as upwelling of Circumpolar Deep Waters, with high  $^{230}\text{Th}$  content, has been previously observed (Rutgers van der Loeff and Berger, 1993; Walter et al., 2000; Chase et al., 2003; Venchiarutti et al., 2008, 2011; Rutgers van der Loeff et al., 2016; Roy-Barman et al., 2019). Therefore, it is necessary to investigate the extent to which vertical mixing can produce an overestimation in the  $^{230}\text{Th}$ -estimated surface residence time over the KP. Rosso et al. (2014) noted that over the shallow areas of the KP, vertical velocities are weak and that the water-motion is dominated mainly by the horizontal component, and it is only on the eastern flank of the plateau where the vertical motion becomes very strong.

As a starting point to constrain the vertical input of  $^{230}\text{Th}$ , we estimate the vertical advective supply of  $^{230}\text{Th}$  by multiplying its concentration at 100 m (or the nearest sample available) by the upwelling velocities reported over ( $0.5 \text{ m day}^{-1}$ ) and on the eastern ( $5 \text{ m day}^{-1}$ ) flank of the plateau respectively (Rosso et al., 2014). Additionally, we calculate the supply of  $^{230}\text{Th}$  through vertical diffusive mixing by multiplying the dissolved  $^{230}\text{Th}$  concentration gradient at  $\sim 100$  m by the vertical mixing coefficient for the plateau ( $K_v = 35 \text{ m}^2 \text{ day}^{-1}$ ; Park et al., 2008a). Using these parameters, we estimate that at Station 16 vertical mixing and upwelling above 100 m could supply an amount of  $^{230}\text{Th}$  equivalent to up 50% of the production rate of  $^{230}\text{Th}$ , which could lead to an overestimation of  $230RT$  by a factor of 1.5. In Stations 6, 9 and 12, located on the eastern flank of the plateau, and in an area that Rosso et al. (2014) suggests having strong vertical velocities, upwelling itself can produce an overestimation of  $230RT$  by a factor of 4 to 10 times.

Another way of investigating the effect of upwelling on the  $230RT$  is by comparing it with the residence time obtained with  $^{234}\text{Th}$  ( $234RT$ ), as its shorter half-life makes it less susceptible to the impact of deep upwelling (Luo et al., 1995). To do so, we have applied Equation 4 to the  $^{234}\text{Th}$  data obtained during the KEOPS 1 voyage (Savoye et al., 2008). Although the samples were not collected in the same year or from exactly the same location, we consider that both datasets were collected close enough and during the same season making a comparison valid (Figure 2). For a comparison of the residence time in the shallow areas of the plateau ( $< 500$  m) we compare Station 16 (HEOBI) to Stations B1 and B5 (KEOPS 1). To compare the residence time on the eastern flank of the plateau, Stations 6, 9, and 12 (HEOBI) are compared to Stations B11 and C11 (KEOPS 1).

The residence time at 100 m obtained with both Th isotopes is almost identical over shallow areas of the plateau (Table 2), confirming the almost neglectable effect of vertical mixing in this area as suggested by Rosso et al. (2014). Surprisingly, in Stations 6, 9 and 12 the  $230RT$  is, at most, 1.5 times higher

**TABLE 2** | Comparison between residence times obtained above 100 m using  $^{230}\text{Th}$  (this study) and  $^{234}\text{Th}$  (Savoye et al., 2008) data from stations located on-plateau and on the eastern flank of the Kerguelen Plateau.

	Station	$^{230}\text{RT}$ [years]	$^{234}\text{RT}$ [years]
On-plateau	16	0.4	–
	B3	–	0.3
	B5	–	0.4
Eastern flank	6	0.5	–
	9	0.6	–
	12	0.6	–
	B11	–	0.4
	C11-Jan	–	0.5
	C11-Feb	–	0.4

than  $^{234}\text{RT}$ . This minor difference between the Th isotopes can be attributed to upwelling, although it is clear that it is not nearly as intense as the 10 times overestimation predicted for this area using the advection parameters. Alternatively, the difference in  $^{230}\text{RT}$  and  $^{234}\text{RT}$  in this area could also reflect different conditions at the time of sampling given that the data are from different years and locations. The use of multiple Th tracers, coupled with an accurate understanding of the physical oceanographic setting of the area, is necessary to fully constrain the scavenging residence time of Th in regions susceptible to deep upwelling.

With increasing depth, the  $^{230}\text{RT}$  increases gradually reflecting the long-term process of  $^{230}\text{Th}$  adsorption and desorption from particles through its path down the water column (Figure 9A; Nozaki et al., 1981; Anderson et al., 1983; Nozaki and Nakanishi, 1985). In particular,  $^{230}\text{RT}$  in the mixed layer is less than a year at all stations (Table 3).

At 500 m the  $^{230}\text{RT}$  reaches more than a year for all stations with the exception of Station 16 at 430 m where it is slightly lower (0.9 years) due to enhanced scavenging of  $^{230}\text{Th}$  by sediments resuspended from the bottom (Figure 5, right panel).

The mixed layer  $^{230}\text{RT}$  values are comparable to those found in the North Pacific (0.7–1.2 years; Hayes et al., 2013), but shorter than residence times calculated from samples collected from the Atlantic Ocean (1.2–2.5 years; Hsieh et al., 2011; Deng et al., 2014). This difference is expected because the Atlantic studies were conducted in a more open oceanic environment with low biological productivity and away from direct sources of particles other than the deposition of aeolian dust. In contrast, the sampled areas of the North Pacific and the KP are closer to particle sources including a larger supply of lithogenic particles to the water column, increasing scavenging rates and shortening  $^{230}\text{RT}$ . However, at 500 m the  $^{230}\text{RT}$  for the KP is considerably shorter than for the Pacific at the same depth (3.3–6.4 years; Hayes et al., 2013) and the Atlantic at 250 m (3.5–6.4 years; Deng et al., 2014). This difference arises very likely because of the shallow bathymetry over the plateau (<500 m) and its interaction with the ACC that generates a dynamic coastal environment, with a continuous supply and resuspension of particles. This larger particle load over the plateau increases scavenging rates, thus shortening residence times.

### Thorium-Derived Lithogenic Fluxes to the Kerguelen Plateau

To obtain an estimation of the flux of lithogenic material using dissolved Th-isotopes it is first necessary to convert  $^{232}\text{Th}$  concentrations into a dissolved flux using the residence time calculated in the previous section. For this, dissolved  $^{232}\text{Th}$  concentrations were integrated from the surface to an integration

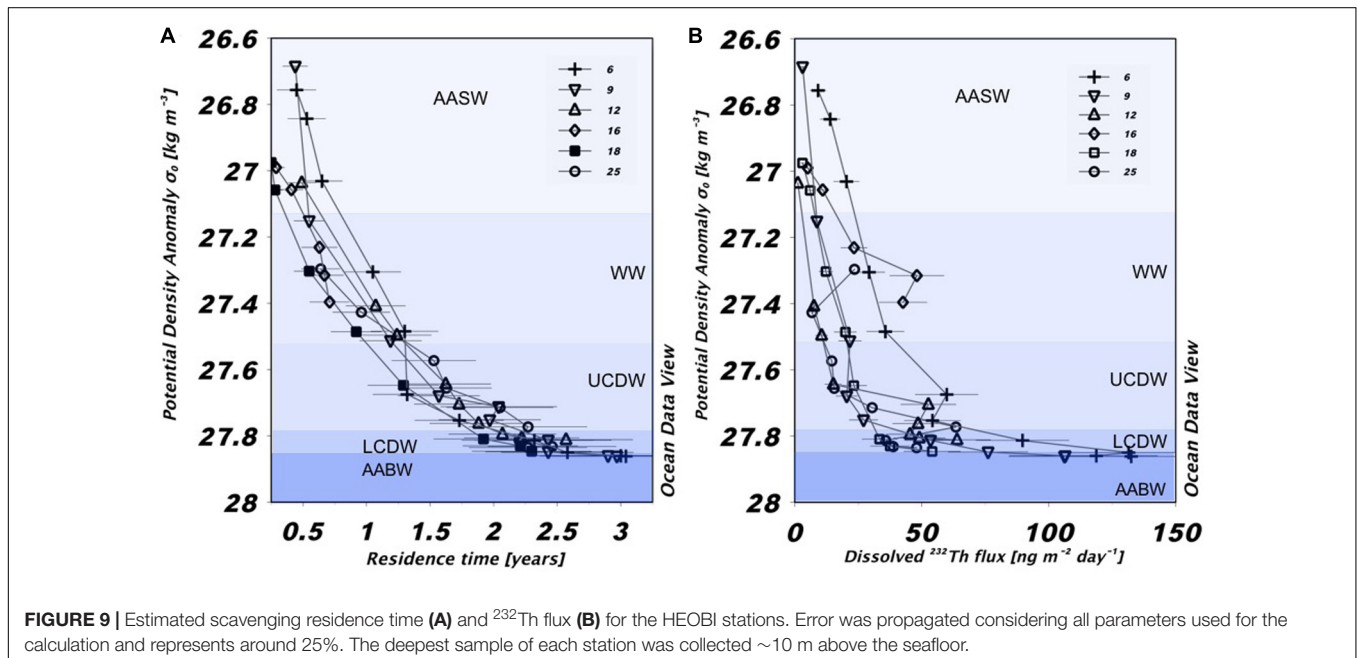




**TABLE 3** | Comparison between residence time and  $^{232}\text{Th}$  fluxes in the mixed layer (ML) depth and at 500 m during the HEOBI voyage.

Station (ML depth)	ML residence time (years)	500 m residence time (years)	ML diss. $^{232}\text{Th}$ flux [ $\text{ng m}^{-2} \text{day}^{-1}$ ]	500 m dissolved $^{232}\text{Th}$ flux [ $\text{ng m}^{-2} \text{day}^{-1}$ ]
6 (110 m)	$0.5 \pm 0.1$	$1.2 \pm 0.2$	$17 \pm 4$	$33 \pm 6$
9 (154 m)	$0.7 \pm 0.1$	$1.4 \pm 0.3$	$9 \pm 2$	$21 \pm 5$
12 (189 m)	$0.8 \pm 0.2$	$1.3 \pm 0.3$	$5 \pm 2$	$12 \pm 3$
16 (181 m)	$0.5 \pm 0.1$	$0.9^* \pm 0.1$	$34 \pm 5$	$43 \pm 9$
18 (282 m)	$0.6 \pm 0.1$	$1.0 \pm 0.2$	$10 \pm 3$	$20 \pm 5$
25 (202 m)	$0.8 \pm 0.1$	$1.3 \pm 0.3$	$24 \pm 5$	$18 \pm 3$

\*The residence time for station 16 was calculated at 430 m because the station had a bottom depth of 446 m. Error has been propagated considering all variables used for the calculation of the residence time and  $^{232}\text{Th}$  flux.

depth and divided by the corresponding  $^{230}\text{Th}$  (Figure 9B; Eq. 5). Selecting an integration depth at which the lithogenic inputs can be effectively quantified has been a subject of discussion. Previous studies aimed mostly to quantify the flux of trace metals originating from the dissolution of mineral dust, therefore Hsieh et al. (2011) integrated only to 25 m, where most of the dust dissolution is expected to occur. However, Hayes et al. (2017) suggests that integration should be done at least to the base of the euphotic zone (50–200 m) in order to capture the effect of Th cycling in the upper layers of the ocean, which is a complex process regulated by particle aggregation, passive sinking and active transport by zooplankton. Furthermore, integrating even deeper (250–500 m), might also account for dissolved Th regeneration below the euphotic zone (Hayes et al., 2017).

In the KP, we expect a source of  $^{232}\text{Th}$  (and Fe) at the ocean surface, from glacial and fluvial runoff. However, given the KP is a “shallow” area (<500 m), plateau-deposited sediments might become an extra source. If  $^{232}\text{Th}$  is supplied to the surface, it would be expected for the  $^{232}\text{Th}$  flux to be higher at the surface, and if no sub-surface source exists, this flux should remain constant with deeper integration. However, in all stations sampled on the KP (except Station 25), we observe an increase in the  $^{232}\text{Th}$  flux from the mixed layer toward 500 m (Table 3), and in general all the way to the bottom. Such an increase in the  $^{232}\text{Th}$  flux with depth has been observed in all of the previous studies where this technique has been applied (Hsieh et al., 2011; Hayes et al., 2013, 2015, 2017; Deng et al., 2014; Lopez et al., 2015; Anderson et al., 2016), and its cause is still not completely understood. Two main hypotheses have been suggested: (1) different chemical speciation between  $^{230}\text{Th}$  and  $^{232}\text{Th}$  that lead to difference in their scavenging rates (Hayes et al., 2013), and (2) irreversible scavenging of both isotopes in the euphotic zone that causes a downward export of Th out of this zone (Hayes et al., 2017). These authors made an important contribution toward explaining the reason for the increase of the  $^{232}\text{Th}$  flux with depth, as they were able to reject the first theory for the Atlantic and the North Pacific and pointed at the second hypothesis as the most likely cause. Therefore, we opt to use an integration depth of 500 m to estimate the lithogenic flux to the plateau, in order to capture all the sub-surface Th cycling and concentration spikes observed in most of the stations. In Station 25, the flux at the base of the mixed layer (202 m;  $23 \text{ ng m}^{-2} \text{ day}^{-1}$ ) is higher than at 100 m ( $12 \text{ ng m}^{-2} \text{ day}^{-1}$ )

and 500 m ( $18 \text{ ng m}^{-2} \text{ day}^{-1}$ ). This elevated value is due to the spike in the  $^{232}\text{Th}$  concentration at this depth (Figure 5), which as we mentioned in the results section could be due to sample contamination, or possibly a shelf-derived sub-surface source of lithogenic material, although turbidity data suggests it's not a local source (Figure 5).

The  $^{232}\text{Th}$  fluxes (Figure 9B) can now be converted to lithogenic-material fluxes with knowledge about the composition of the material and its Th fractional solubility (Eq. 5). In other words, this flux of lithogenic material is required to sustain the calculated dissolved  $^{232}\text{Th}$  fluxes and therefore measured concentrations of  $^{232}\text{Th}$ . Previous studies dedicated to quantifying the input of dust to the ocean have used the average  $^{232}\text{Th}$  concentration for the upper continental crust that can range from 10.5 to 14.6 ppm (Taylor and McLennan, 1985; Rudnick and Gao, 2013; Serno et al., 2014). The lithogenic material from the volcanic KP province has a lower  $^{232}\text{Th}$  content than average continental crust ( $5.4 \pm 1.5 \text{ ppm}$ ; Duncan et al., 2016; Fox, 2019, personal communication). Therefore, we use this value for the calculations of the lithogenic flux in our area of study.

The largest source of uncertainty in the calculation of lithogenic fluxes is the solubility of  $^{232}\text{Th}$  from particles, which is a highly unconstrained parameter, especially for volcanic-derived material. From the few studies that report  $^{232}\text{Th}$  solubility in marine particles, highly variable values were found, ranging from 1 to 23%, depending on the particle size and depth (Arraes-Mescoff et al., 2001; Roy-Barman et al., 2002). When using a Th solubility of 1% we obtain fluxes of lithogenic material that range from  $144$  to  $810 \text{ mg m}^{-2} \text{ day}^{-1}$  in the top 500 m of the water column, while the values range from  $7$  to  $39 \text{ mg m}^{-2} \text{ day}^{-1}$  when using a Th solubility from particles of 20% (Table 4).

The dissolved thorium based lithogenic flux estimates for the KP are much higher than sediment-trap based estimates reported in a transect along the Southwest sector of the Pacific Ocean (Honjo et al., 2000). This difference is consistent with the oceanic setting of the transect in the Pacific Ocean at 170 W, distant from any significant lithogenic source. Our calculated lithogenic fluxes are however comparable to sediment-trap obtained fluxes reported for more “coastal” parts of the Southern Ocean like the Ross Sea (Chiarini et al., 2019) and the Bransfield Strait (Wefer et al., 1988). Furthermore, all of our Th-derived lithogenic fluxes fall within the range reported for the KP using drifting



**TABLE 4** | Comparison of the Th-derived lithogenic and dissolved Fe fluxes to those reported in the literature.

Area of study	Th-litho. flux $S_{Th} = 1\%^a$	Th-litho. flux $S_{Th} = 20\%^a$	Sed. trap litho flux <sup>a</sup>	dFe flux <sup>b</sup>	Non-litho Fe export flux <sup>b</sup>
KP-shallow (HEOBI)	586–810	23–40	–	4,189–6,800	–
KP-eastern flank (HEOBI)	230–617	11–30	–	1,400–4,700	–
KP-shallow KEOPS 2 <sup>c</sup>	–	–	35–625	1,342	2,797
Ross Sea <sup>d</sup>	–	–	26–148	–	–
Southern Ocean, along 170°W <sup>e</sup>	–	–	0.14–2	–	–
Bransfield Strait, Ant. Peninsula <sup>f</sup>	–	–	8.4–777	–	–

The table also includes a comparison of the dissolved Fe fluxes estimated with Th long-lived isotopes against the fluxes obtained at Station A3 during the KEOPS 2 voyage. Lithogenic flux from KEOPS 2 was calculated as: Lithogenic flux = Total mass flux – (bioSiO<sub>2</sub> + PIC + POM). <sup>a</sup>mg m<sup>-2</sup> day<sup>-1</sup>; <sup>b</sup>nmol m<sup>-2</sup> day<sup>-1</sup>; <sup>c</sup>Bowie et al., 2015; <sup>d</sup>Chiarini et al., 2019; <sup>e</sup>Honjo et al., 2000; <sup>f</sup>Wefer et al., 1988.

sediment traps (Table 4; Bowie et al., 2015). Lithogenic material flux calculation using thorium isotopes for coastal areas seems to be promising and once the Th solubility in the plateau is better constrained, the uncertainties will be reduced.

## Quantification of Fe Fluxes to the Plateau

In a similar manner to the previous section, <sup>232</sup>Th fluxes can be used to derive fluxes of dissolved Fe and other trace elements from lithogenic material. For this, information about the metal concentration in lithogenic particles and their solubility relative to that of <sup>232</sup>Th is required (Eq. 7). Unfortunately, the solubility of trace elements with respect to <sup>232</sup>Th has so far not been reported. However, it has been suggested that over time, relatively insoluble elements (such as Th and Fe) tend to present a similar solubility (Hayes et al., 2013). Therefore, we can expect that Fe and <sup>232</sup>Th should have similar solubilities (Fe/<sup>232</sup>Th ≈ 1), however it's necessary to mention that the residence time of Fe in the region is still not completely constrained. Making this assumption and considering an average Fe/<sup>232</sup>Th ratio of lithogenic material over the shallow areas of the plateau of 16,400 g g<sup>-1</sup> (Duncan et al., 2016; Fox, 2019, personal communication), we obtain dissolved Fe fluxes at the base of the mixed layer at stations located over the KP that range from 4,200 to 6,800 nmol m<sup>-2</sup> day<sup>-1</sup>. Such amount of Fe is higher than the estimates produced from the dissolution of natural mineral dust in the Northern Pacific Ocean (245–736 nmol m<sup>-2</sup> day<sup>-1</sup>; Hayes et al., 2013). This is because of the higher flux of lithogenic particles in our area of study, and increased content of Fe in the basalts from the KP.

This dissolved Fe supply from the dissolution of lithogenic material can be compared to Bowie et al. (2015)'s estimate of the dissolved Fe supply to the mixed layer at station A3 (Figure 1), sampled during the KEOPS 2 voyage (Table 4). They estimate a dissolved Fe supply of 1,342 nmol m<sup>-2</sup> day<sup>-1</sup>, from total vertical and lateral advective supply (1,292 nmol m<sup>-2</sup> day<sup>-1</sup>), and atmospheric soluble deposition (50 nmol m<sup>-2</sup> day<sup>-1</sup>). It becomes evident that the estimates of our study are more than three times larger than the previously estimated supply of dissolved Fe above the plateau. Furthermore, Bowie et al. (2015) noted that at station A3, on the plateau (relatively close to our station 16), the export of particulate non-lithogenic Fe from the mixed layer (2,797 nmol m<sup>-2</sup> day<sup>-1</sup>) exceeded the estimated supply of dissolved Fe (1,342 nmol m<sup>-2</sup> day<sup>-1</sup>). This suggests the scavenging and biological removal of Fe from the mixed layer is

greater than the rate of supply of dissolved Fe. Hence, there must be at least one source of Fe that has not been taken into account. The same authors and Chever et al. (2010) noted that this extra source is very likely from lithogenic particulate Fe, derived from either the Kerguelen plateau or the HIMI region, that might be converted into dissolved and bio-available Fe. This hypothesis is supported by recent findings of van der Merwe et al. (2019), who claimed that high-lability Fe particles sourced from glacial erosion from Heard Island might be this missing source of iron. Our dissolved Fe estimations, obtained independently through the use of Th isotopes, support this claim as our larger estimate is very likely reflecting the dissolution of Fe from these highly labile particles. Furthermore, our dissolved Fe supply flux estimates are very similar to the total downward particulate Fe export flux (5,746 nmol m<sup>-2</sup> day<sup>-1</sup>) reported by Bowie et al. (2015). Although both terms are not directly comparable, our estimates might help to close the iron budget of the KP, implicating the dissolution of lithogenic particles from HIMI as a major source of dissolved Fe to this region.

## CONCLUSION

The spatial distribution of <sup>232</sup>Th concentrations near the surface of the plateau clearly indicate that Heard and McDonald Islands contribute to the supply of lithogenic material that fuels the phytoplankton bloom in the central KP during the summer. We applied long-lived Th isotopes to produce an estimation of the fluxes of lithogenic material and Fe in the KP. We demonstrate the potential of long-lived Th isotopes to produce this type of information not only from the dissolution of aeolian dust to the open ocean, like other studies have shown, but also from the input of lithogenic sources to coastal areas. The similarity of our results with those obtained using sediment traps in the SO suggests that measuring Th isotopes can be an alternative approach to obtain this type of information, and can also provide greater spatial detail than sediment traps. However, some limitations arise due to the lack of information about the solubility of Th. Systematic studies about these parameters in particles of different origin and composition will improve the results produced by this approach. Nevertheless, our results help to close the iron budget in this region, and confirm that the release of iron from the dissolution of lithogenic particles is a key source of soluble iron to support biological activity on the KP.

## DATA AVAILABILITY STATEMENT

All datasets generated for this study are included in the article/**Supplementary Material**.

## AUTHOR CONTRIBUTIONS

HP-T and ZC collected the samples. HP-T processed and analyzed the samples, interpreted the results and prepared the first version of the manuscript. ZC and TN contributed to the data interpretation and provided comments for the manuscript. AT and AB provided suggestions to the final version of the manuscript. AT supported the analysis on the SF-ICP-MS.

## FUNDING

This work was supported by the following grants: Australian Research Council Discovery (DP150100345 and DP180102357), Australian Research Council LIEF (LF0989539), the Australian Antarctic Science Program (AAS4338) and the Australian Research Council Special Research Initiative for Antarctic

## REFERENCES

- Andersen, M. B., Stirling, C. H., Zimmermann, B., and Halliday, A. N. (2010). Precise determination of the open ocean 234U/238U composition. *Geochem. Geophys. Geosyst.* 11. doi: 10.1029/2010GC003318
- Anderson, R. F., Bacon, M. P., and Brewer, P. G. (1983). Removal of 230Th and 231Pa from the open ocean. *Earth Planet. Sci. Lett.* 62, 7–23. doi: 10.1016/0012-821X(83)90067-5
- Anderson, R. F., Cheng, H., Edwards, R. L., Fleisher, M. Q., Hayes, C. T., Huang, K.-F., et al. (2016). How well can we quantify dust deposition to the ocean? *Philos. Trans. R. Soc. A Math. Phys. Eng. Sci.* 374:20150285. doi: 10.1098/rsta.2015.0285
- Anderson, R. F., Fleisher, M. Q., Robinson, L. F., Edwards, R. L., Hoff, J. A., Moran, S. B., et al. (2012). GEOTRACES intercalibration of 230Th, 232Th, 231Pa, and prospects for 10Be. *Limnol. Oceanogr. Methods* 10, 179–213. doi: 10.4319/lom.2012.10.179
- Arraes-Mescoff, R., Roy-Barman, M., Coppola, L., Souhaut, M., Tachikawa, K., Jeandel, C., et al. (2001). The behavior of Al, Mn, Ba, Sr, REE and Th isotopes during in vitro degradation of large marine particles. *Mar. Chem.* 73, 1–19. doi: 10.1016/S0304-4203(00)00065-7
- Beaman, R. J., and O'Brien, P. E. (2011). Kerguelen Plateau Bathymetric Grid, November 2010. Record 2011/22. *Geosci. Aust. Canberra Aust.* 18.
- Blain, S., Quéguiner, B., Armand, L., Belviso, S., Bombled, B., Bopp, L., et al. (2007). Effect of natural iron fertilization on carbon sequestration in the Southern Ocean. *Nature* 446, 1070–1074. doi: 10.1038/nature05700
- Blain, S., Quéguiner, B., and Trull, T. (2008a). The natural iron fertilization experiment KEOPS (Kerguelen Ocean and Plateau compared Study): an overview. *Deep Sea Res. Part II Top. Stud. Oceanogr.* 55, 559–565. doi: 10.1016/j.dsr2.2008.01.002
- Blain, S., Sarthou, G., and Laan, P. (2008b). Distribution of dissolved iron during the natural iron-fertilization experiment KEOPS (Kerguelen Plateau, Southern Ocean). *Deep Sea Res. Part II Top. Stud. Oceanogr.* 55, 594–605. doi: 10.1016/j.dsr2.2007.12.028
- Blain, S., Tréguer, P., Belviso, S., Bucciarelli, E., Denis, M., Desabre, S., et al. (2001). A biogeochemical study of the island mass effect in the context of the iron hypothesis: Kerguelen Islands, Southern Ocean. *Deep Sea Res. Part I Oceanogr. Res. Pap.* 48, 163–187. doi: 10.1016/S0967-0637(00)00047-9

Gateway Partnership (Project ID SR140300001). This research was supported by the Science and Industry Endowment Fund.

## ACKNOWLEDGMENTS

We are very grateful for the invaluable contributions from the reviewers which helped to greatly improve this article. We also thank the CSIRO Marine National Facility (MNF) for ship time support on the RV Investigator voyage IN2016\_V01 (HEOBI). We thank the captain, crew, support personnel, data managers, and chief scientist Mike Coffin for their excellent help. We also thank Tom Trull, Pier van Der Merwe, and Jodi Fox for their comments and ideas during the HEOBI discussion meetings, and to IMAS trace metal lab manager Pam Quayle for her logistic support.

## SUPPLEMENTARY MATERIAL

The Supplementary Material for this article can be found online at: <https://www.frontiersin.org/articles/10.3389/fmars.2020.00207/full#supplementary-material>

- Bopp, L., Aumont, O., Belviso, S., and Blain, S. (2008). Modelling the effect of iron fertilization on dimethylsulphide emissions in the Southern Ocean. *Deep Sea Res. Part II Top. Stud. Oceanogr.* 55, 901–912. doi: 10.1016/j.dsr2.2007.12.002
- Bowie, A. R., van der Merwe, P., Quéroué, F., Trull, T., Fourquez, M., Planchon, F., et al. (2015). Iron budgets for three distinct biogeochemical sites around the Kerguelen Archipelago (Southern Ocean) during the natural fertilisation study, KEOPS-2. *Biogeosciences* 12, 4421–4445. doi: 10.5194/bg-12-4421-2015
- Bown, J., Boye, M., Laan, P., Bowie, A. R., Park, Y.-H., Jeandel, C., et al. (2012). Imprint of a dissolved cobalt basaltic source on the Kerguelen Plateau. *Biogeosciences* 9, 5279–5290. doi: 10.5194/bg-9-5279-2012
- Boyd, P. W., and Ellwood, M. J. (2010). The biogeochemical cycle of iron in the ocean. *Nat. Geosci.* 3, 675–682. doi: 10.1038/ngeo964
- Boyd, P. W., Jickells, T., Law, C. S., Blain, S., Boyle, E. A., Buesseler, K. O., et al. (2007). Mesoscale iron enrichment experiments 1993–2005: synthesis and future directions. *Science* 315, 612–617. doi: 10.1126/science.1131669
- Broecker, W. S., Kaufman, A., and Trier, R. M. (1973). The residence time of thorium in surface sea water and its implications regarding the rate of reactive pollutants. *Earth Planet. Sci. Lett.* 20, 35–44. doi: 10.1016/0012-821X(73)90137-4
- Buesseler, K. O., Bacon, M. P., Kirk Cochran, J., and Livingston, H. D. (1992). Carbon and nitrogen export during the JGOFS North Atlantic bloom experiment estimated from 234Th: 238U disequilibria. *Deep Sea Res. Part A. Oceanogr. Res. Pap.* 39, 1115–1137. doi: 10.1016/0198-0149(92)90060-7
- Chase, Z., Anderson, R. F., Fleisher, M. Q., and Kubik, P. W. (2003). Scavenging of 230Th, 231Pa and 10Be in the Southern Ocean (SW Pacific sector): the importance of particle flux, particle composition and advection. *Deep Res. Part II Top. Stud. Oceanogr.* 50, 739–768. doi: 10.1016/S0967-0645(02)00593-3
- Chever, F., Sarthou, G., Bucciarelli, E., Blain, S., and Bowie, A. R. (2010). An iron budget during the natural iron fertilisation experiment KEOPS (Kerguelen Islands, Southern Ocean). *Biogeosciences* 7, 455–468. doi: 10.5194/bg-7-455-2010
- Chiarini, F., Ravaioli, M., and Capotondi, L. (2019). Interannual variability of vertical particle fluxes in the Ross Sea (Antarctica). *Nat. Conserv.* 34, 417–440. doi: 10.3897/natureconservation.34.30732
- Cochran, J. K., Buesseler, K. O., Bacon, M. P., Wang, H. W., Hirschberg, D. J., Ball, L., et al. (2000). Short-lived thorium isotopes (234Th, 228Th) as indicators of POC export and particle cycling in the Ross Sea, Southern Ocean. *Deep Sea*

- Res. Part II Top. Stud. Oceanogr. 47, 3451–3490. doi: 10.1016/S0967-0645(00)00075-8
- Coppola, L., Roy-Barman, M., Mulrow, S., Povinec, P., and Jeandel, C. (2006). Thorium isotopes as tracers of particles dynamics and deep water circulation in the Indian sector of the Southern Ocean (ANTARES IV). *Mar. Chem.* 100, 299–313. doi: 10.1016/j.marchem.2005.10.019
- Costa, K., and McManus, J. (2017). Efficacy of  $^{230}\text{Th}$  normalization in sediments from the Juan de Fuca Ridge, northeast Pacific Ocean. *Geochim. Cosmochim. Acta* 197, 215–225. doi: 10.1016/j.gca.2016.10.034
- Deng, F., Thomas, A. L., Rijkbergen, M. J. A., and Henderson, G. M. (2014). Controls on seawater  $^{231}\text{Pa}$ ,  $^{230}\text{Th}$  and  $^{232}\text{Th}$  concentrations along the flow paths of deep waters in the Southwest Atlantic. *Earth Planet. Sci. Lett.* 390, 93–102. doi: 10.1016/j.epsl.2013.12.038
- Duncan, R. A., Falloon, T. J., Quilty, P. G., and Coffin, M. F. (2016). Widespread Neogene volcanism on Central Kerguelen Plateau, Southern Indian Ocean. *Aust. J. Earth Sci.* 63, 379–392. doi: 10.1080/08120099.2016.1221857
- Francois, R., Bacon, M. P., and Suman, D. O. (1990). Thorium 230 profiling in deep-sea sediments: high-resolution records of flux and dissolution of carbonate in the equatorial Atlantic during the last 24,000 years. *Paleoceanography* 5, 761–787. doi: 10.1029/PA005i005p00761
- Francois, R., Frank, M., Rutgers van der Loeff, M. M., and Bacon, M. P. (2004).  $^{230}\text{Th}$  normalization: an essential tool for interpreting sedimentary fluxes during the late Quaternary. *Paleoceanography* 19. doi: 10.1029/2003PA000939
- Fung, I. Y., Meyn, S. K., Tegen, I., Doney, S. C., John, J. G., and Bishop, J. K. B. (2000). Iron supply and demand in the upper ocean. *Glob. Biogeochem. Cycles* 14, 281–295. doi: 10.1029/1999GB900059
- Grenier, M., Garcia-Solsona, E., Lemaitre, N., Trull, T. W., Bouvier, V., Nonnotte, P., et al. (2018). Differentiating lithogenic supplies, water mass transport, and biological processes on and off the kerguelen plateau using rare earth element concentrations and neodymium isotopic compositions. *Front. Mar. Sci.* 5:426. doi: 10.3389/fmars.2018.00426
- Hayes, C. T., Anderson, R. F., Fleisher, M. Q., Serno, S., Winckler, G., and Gersonde, R. (2013). Quantifying lithogenic inputs to the North Pacific Ocean using the long-lived thorium isotopes. *Earth Planet. Sci. Lett.* 383, 16–25. doi: 10.1016/j.epsl.2013.09.025
- Hayes, C. T., Black, E. E., Anderson, R. F., Baskaran, M., Buesseler, K. O., Charette, M. A., et al. (2018). Flux of particulate elements in the north atlantic ocean constrained by multiple radionuclides. *Glob. Biogeochem. Cycles* 32, 1738–1758. doi: 10.1029/2018GB005994
- Hayes, C. T., Fitzsimmons, J. N., Boyle, E. A., McGee, D., Anderson, R. F., Weisend, R., et al. (2015). Thorium isotopes tracing the iron cycle at the Hawaii Ocean time-series station ALOHA. *Geochim. Cosmochim. Acta* 169, 1–16. doi: 10.1016/j.gca.2015.07.019
- Hayes, C. T., Rosen, J., McGee, D., and Boyle, E. A. (2017). Thorium distributions in high- and low-dust regions and the significance for iron supply. *Glob. Biogeochem. Cycles* 31, 1–20. doi: 10.1002/2016GB005511
- Holmes, T. M., Wuttig, K., Chase, Z., van der Merwe, P., Townsend, A. T., Schallenberg, C., et al. (2019). Iron availability influences nutrient drawdown in the Heard and McDonald Islands region, Southern Ocean. *Mar. Chem.* 211, 1–14. doi: 10.1016/j.marchem.2019.03.002
- Honjo, S., Francois, R., Manganini, S., Dymond, J., and Collier, R. (2000). Particle fluxes to the interior of the Southern Ocean in the Western Pacific sector along  $170^\circ\text{W}$ . *Deep Sea Res. Part II Top. Stud. Oceanogr.* 47, 3521–3548. doi: 10.1016/S0967-0645(00)00077-1
- Hsieh, Y., Henderson, G. M., and Thomas, A. L. (2011). Combining seawater  $^{232}\text{Th}$  and  $^{230}\text{Th}$  concentrations to determine dust fluxes to the surface ocean. *Earth Planet. Sci. Lett.* 312, 280–290. doi: 10.1016/j.epsl.2011.10.022
- Jacquet, S. H. M., Dehairs, F., Savoye, N., Obernosterer, I., Christaki, U., Monnin, C., et al. (2008). Mesopelagic organic carbon remineralization in the Kerguelen Plateau region tracked by biogenic particulate Ba. *Deep Sea Res. Part II Top. Stud. Oceanogr.* 55, 868–879. doi: 10.1016/j.dsr2.2007.12.038
- Jickells, T. D. (2005). Global iron connections between desert dust, ocean biogeochemistry, and climate. *Science* 308, 67–71. doi: 10.1126/science.1105959
- Jouandet, M. P., Blain, S., Metzler, N., Brunet, C., Trull, T. W., and Obernosterer, I. (2008). A seasonal carbon budget for a naturally iron-fertilized bloom over the Kerguelen Plateau in the Southern Ocean. *Deep Sea Res. Part II Top. Stud. Oceanogr.* 55, 856–867. doi: 10.1016/j.dsr2.2007.12.037
- Krishnaswami, S., and Cochran, J. K. (2011). *U-Th Series Nuclides in Aquatic Systems*. Amsterdam: Elsevier.
- Krishnaswami, S., and Cochran, J. K. (2008). *Radioactivity in the Environment*. Amsterdam: Elsevier, 1–10.
- Lopez, G. I., Marcantonio, F., Lyle, M., and Lynch-Stieglitz, J. (2015). Dissolved and particulate  $^{230}\text{Th}$ - $^{232}\text{Th}$  in the Central Equatorial Pacific Ocean: evidence for far-field transport of the East Pacific Rise hydrothermal plume. *Earth Planet. Sci. Lett.* 431, 87–95. doi: 10.1016/j.epsl.2015.09.019
- Luo, S., Ku, T. L., Kusakabe, M., Bishop, J. K. B., and Yang, Y. L. (1995). Tracing particle cycling in the upper ocean with  $^{230}\text{Th}$  and  $^{228}\text{Th}$ : an investigation in the equatorial Pacific along  $140^\circ\text{W}$ . *Deep Sea Res. Part II* 42, 805–829. doi: 10.1016/0967-0645(95)00019-M
- Luo, Y. (2017). Reinterpretation of oceanic  $^{230}\text{Th}$  profiles based on decadal export productivity (2003–2010). *Sci. Rep.* 7:505. doi: 10.1038/s41598-017-00604-y
- Mahowald, N., Engelstaedter, S., and Luo, C. (2009). Atmospheric iron deposition: global distribution, variability, and human perturbations. *Annu. Rev. Mar. Sci.* 1, 245–278. doi: 10.1146/annurev.marine.010908.163727
- Martin, J. H. (1990). Glacial-interglacial  $\text{CO}_2$  change: the iron hypothesis. *Paleoceanography* 5, 1–13. doi: 10.1029/PA005i001p00001
- Mongin, M., Molina, E., and Trull, T. W. (2008). Seasonality and scale of the Kerguelen plateau phytoplankton bloom: a remote sensing and modeling analysis of the influence of natural iron fertilization in the Southern Ocean. *Deep Sea Res. Part II Top. Stud. Oceanogr.* 55, 880–892. doi: 10.1016/j.dsr2.2007.12.039
- Moore, C. M., Mills, M. M., Arrigo, K. R., Berman-Frank, I., Bopp, L., Boyd, P. W., et al. (2013). Processes and patterns of oceanic nutrient limitation. *Nat. Geosci.* 6, 701–710. doi: 10.1038/ngeo1765
- Moran, S. B., Shen, C.-C., Edmonds, H. N., Weinstein, S. E., Smith, J. N., and Edwards, R. L. (2002). Dissolved and particulate  $^{231}\text{Pa}$  and  $^{230}\text{Th}$  in the Atlantic Ocean: constraints on intermediate/deep water age, boundary scavenging, and  $^{231}\text{Pa}/^{230}\text{Th}$  fractionation. *Earth Planet. Sci. Lett.* 203, 999–1014. doi: 10.1016/S0012-821X(02)00928-7
- Morris, P. J., and Charette, M. A. (2013). A synthesis of upper ocean carbon and dissolved iron budgets for Southern Ocean natural iron fertilisation studies. *Deep Sea Res. Part II Top. Stud. Oceanogr.* 90, 147–157. doi: 10.1016/j.dsr2.2013.02.001
- Mosseri, J., Quéguiner, B., Armand, L., and Cornet-Barthaux, V. (2008). Impact of iron on silicon utilization by diatoms in the Southern Ocean: a case study of Si/N cycle decoupling in a naturally iron-enriched area. *Deep Sea Res. Part II Top. Stud. Oceanogr.* 55, 801–819. doi: 10.1016/j.dsr2.2007.12.003
- Nozaki, Y., Horibe, Y., and Tsubota, H. (1981). The water column distributions of thorium isotopes in the western North Pacific. *Earth Planet. Sci. Lett.* 54, 203–216. doi: 10.1016/0012-821X(81)90004-2
- Nozaki, Y., and Nakanishi, T. (1985).  $^{231}\text{Pa}$  and  $^{230}\text{Th}$  profiles in the open ocean water column. *Deep Sea Res. Part A. Oceanogr. Res. Pap.* 32, 1209–1220. doi: 10.1016/0198-0149(85)90004-4
- Owens, S. A., Buesseler, K. O., and Sims, K. W. W. (2011). Re-evaluating the  $^{238}\text{U}$ -salinity relationship in seawater: implications for the  $^{238}\text{U}$ - $^{234}\text{Th}$  disequilibrium method. *Mar. Chem.* 127, 31–39. doi: 10.1016/j.marchem.2011.07.005
- Park, Y., and Vivier, F. (2011). Circulation and hydrography over the Kerguelen Plateau. *Kerguelen Plateau Mar. Ecosyst. Fish.* 35, 43–55.
- Park, Y.-H., Charriaud, E., and Fioux, M. (1998). Thermohaline structure of the Antarctic surface water/winter water in the Indian sector of the Southern Ocean. *J. Mar. Syst.* 17, 5–23. doi: 10.1016/S0924-7963(98)00026-8
- Park, Y.-H., Durand, I., Kestenare, E., Rougier, G., Zhou, M., D'Ovidio, F., et al. (2014). Polar front around the Kerguelen Islands: an up-to-date determination and associated circulation of surface/subsurface waters. *J. Geophys. Res. Ocean.* 119, 6575–6592. doi: 10.1002/2014JC010061
- Park, Y.-H., Fuda, J.-L., Durand, I., and Naveira Garabato, A. C. (2008a). Internal tides and vertical mixing over the Kerguelen Plateau. *Deep Sea Res. Part II Top. Stud. Oceanogr.* 55, 582–593. doi: 10.1016/j.dsr2.2007.12.027
- Park, Y.-H., Roquet, F., Durand, I., and Fuda, J.-L. (2008b). Large-scale circulation over and around the Northern Kerguelen Plateau. *Deep Sea Res. Part II Top. Stud. Oceanogr.* 55, 566–581. doi: 10.1016/j.dsr2.2007.12.030

- Pérez-Tribouillier, H., Noble, T. L., Townsend, A. T., Bowie, A. R., and Chase, Z. (2019). Pre-concentration of thorium and neodymium isotopes using Nobias chelating resin: method development and application to chromatographic separation. *Talanta* 202, 600–609. doi: 10.1016/j.talanta.2019.03.086
- Planchon, F., Ballas, D., Cavagna, A.-J., Bowie, A. R., Davies, D., Trull, T., et al. (2015). Carbon export in the naturally iron-fertilized Kerguelen area of the Southern Ocean based on the 234 Th approach. *Biogeosciences* 12, 3831–3848. doi: 10.5194/bg-12-3831-2015
- Rosso, I., Hogg, A. M. C., Strutton, P. G., Kiss, A. E., Matear, R., Klocker, A., et al. (2014). Vertical transport in the ocean due to sub-mesoscale structures: impacts in the Kerguelen region. *Ocean Model.* 80, 10–23. doi: 10.1016/j.ocemod.2014.05.001
- Roy-Barman, M., Coppola, L., and Souhaut, M. (2002). Thorium isotopes in the western Mediterranean Sea: an insight into the marine particle dynamics. *Earth Planet. Sci. Lett.* 196, 161–174. doi: 10.1016/S0012-821X(01)00606-9
- Roy-Barman, M., Lemaître, C., Ayrault, S., Jeandel, C., Souhaut, M., and Miquel, J. C. (2009). The influence of particle composition on Thorium scavenging in the Mediterranean Sea. *Earth Planet. Sci. Lett.* 286, 526–534. doi: 10.1016/j.epsl.2009.07.018
- Roy-Barman, M., Thil, F., Bordier, L., Dapoigny, A., Foliot, L., Ayrault, S., et al. (2019). Thorium isotopes in the Southeast Atlantic Ocean: tracking scavenging during water mass mixing along neutral density surfaces. *Deep Res. Part I Oceanogr. Res. Pap.* 149:103042. doi: 10.1016/j.dsr.2019.05.002
- Rudnick, R., and Gao, S. (2013). Composition of the continental crust. *Treatise Geochem. Second Ed.* 4, 1–51. doi: 10.1016/B978-0-08-095975-7.00301-6
- Rutgers van der Loeff, M., Venchiarutti, C., Stimac, I., van Ooijen, J., Huhn, O., Rohardt, G., et al. (2016). Meridional circulation across the Antarctic Circumpolar Current serves as a double 231Pa and 230Th trap. *Earth Planet. Sci. Lett.* 455, 73–84. doi: 10.1016/j.epsl.2016.07.027
- Rutgers van der Loeff, M. M., and Berger, G. W. (1993). Scavenging of 230Th and 231Pa near the antarctic polar front in the South Atlantic. *Deep Sea Res. Part I Oceanogr. Res. Pap.* 40, 339–357. doi: 10.1016/0967-0637(93)90007-P
- Sanial, V., van Beek, P., Lansard, B., Souhaut, M., Kestenare, E., Ovidio, F., et al. (2015). Use of Ra isotopes to deduce rapid transfer of sediment-derived inputs off Kerguelen. *Biogeosciences* 12, 1415–1430. doi: 10.5194/bg-12-1415-2015
- Santschi, P. H., Murray, J. W., Baskaran, M., Benitez-Nelson, C. R., Guo, L. D., Hung, C.-C., et al. (2006). Thorium speciation in seawater. *Mar. Chem.* 100, 250–268. doi: 10.1016/j.marchem.2005.10.024
- Sargent, M., Harte, R., and Harrington, C. (2002). *Guidelines for Achieving High Accuracy in Isotope Dilution Mass Spectrometry (IDMS)*. Available online at: [https://books.google.com/books?hl=es&lr=&id=9wwLS5pcD9sC&oi=fnd&pg=PA1&dq=guidelines+for+achieving+high+accuracy+in+isotope+dilution&ots=TI80X664yI&sig=-NVdYoYJtnc\\_SarNw4UVRm1L2jo](https://books.google.com/books?hl=es&lr=&id=9wwLS5pcD9sC&oi=fnd&pg=PA1&dq=guidelines+for+achieving+high+accuracy+in+isotope+dilution&ots=TI80X664yI&sig=-NVdYoYJtnc_SarNw4UVRm1L2jo)
- Sarthou, G., Baker, A. R., Kramer, J., Laan, P., Laës, A., Ussher, S., et al. (2007). Influence of atmospheric inputs on the iron distribution in the subtropical North-East Atlantic Ocean. *Mar. Chem.* 104, 186–202. doi: 10.1016/j.marchem.2006.11.004
- Sarthou, G., Vincent, D., Christaki, U., Obernosterer, I., Timmermans, K. R., and Brussaard, C. P. D. (2008). The fate of biogenic iron during a phytoplankton bloom induced by natural fertilisation: impact of copepod grazing. *Deep Sea Res. Part II Top. Stud. Oceanogr.* 55, 734–751. doi: 10.1016/j.dsr2.2007.12.033
- Savoie, N., Trull, T. W., Jacquet, S. H. M., Navez, J., and Dehairs, F. (2008). 234Th-based export fluxes during a natural iron fertilization experiment in the Southern Ocean (KEOPS). *Deep Sea Res. Part II Top. Stud. Oceanogr.* 55, 841–855. doi: 10.1016/j.dsr2.2007.12.036
- Serno, S., Winckler, G., Anderson, R. F., Hayes, C. T., McGee, D., Machalett, B., et al. (2014). Eolian dust input to the Subarctic North Pacific. *Earth Planet. Sci. Lett.* 387, 252–263. doi: 10.1016/j.epsl.2013.11.008
- Tagliabue, A., Bopp, L., and Aumont, O. (2009). Evaluating the importance of atmospheric and sedimentary iron sources to Southern Ocean biogeochemistry. *Geophys. Res. Lett.* 36:L13601. doi: 10.1029/2009GL038914
- Tagliabue, A., Sallée, J.-B., Bowie, A. R., Lévy, M., Swart, S., and Boyd, P. W. (2014). Surface-water iron supplies in the Southern Ocean sustained by deep winter mixing. *Nat. Geosci.* 7, 314–320. doi: 10.1038/ngeo2101
- Taylor, S. R., and McLennan, S. M. (1985). *The Continental Crust: Its Composition and Evolution*. Hoboken, NJ: Blackwell Scientific Publications.
- Trimble, S. M., Baskaran, M., and Porcelli, D. (2004). Scavenging of thorium isotopes in the Canada Basin of the Arctic Ocean?. *Earth Planet. Sci. Lett.* 222, 915–932. doi: 10.1016/j.epsl.2004.03.027
- Tyrrill, T., Merico, A., Wanek, J. J., Wong, C. S., Metzl, N., and Whitney, F. (2005). Effect of seafloor depth on phytoplankton blooms in high-nitrate, low-chlorophyll (HNLC) regions. *J. Geophys. Res. Biogeosci.* 110. doi: 10.1029/2005JG000041
- van Beek, P., Bourquin, M., Reyss, J.-L., Souhaut, M., Charette, M. A., and Jeandel, C. (2008). Radium isotopes to investigate the water mass pathways on the Kerguelen Plateau (Southern Ocean). *Deep Sea Res. Part II Top. Stud. Oceanogr.* 55, 622–637. doi: 10.1016/j.dsr2.2007.12.025
- van der Merwe, P., Bowie, A. R., Quéroué, F., Armand, L., Blain, S., Chever, F., et al. (2015). Sourcing the iron in the naturally fertilised bloom around the Kerguelen Plateau: particulate trace metal dynamics. *Biogeosciences* 12, 739–755. doi: 10.5194/bg-12-739-2015
- van der Merwe, P., Wuttig, K., Holmes, T., Trull, T. W., Chase, Z., Townsend, A. T., et al. (2019). High lability Fe particles sourced from glacial erosion can meet previously unaccounted biological demand: Heard Island, Southern Ocean. *Front. Mar. Sci.* 6:332. doi: 10.3389/fmars.2019.00332
- Venchiarutti, C., Jeandel, C., and Roy-Barman, M. (2008). Particle dynamics study in the wake of Kerguelen Island using thorium isotopes. *Deep Sea Res. Part I Oceanogr. Res. Pap.* 55, 1343–1363. doi: 10.1016/j.dsr.2008.05.015
- Venchiarutti, C., van der Loeff, M. R., and Stimac, I. (2011). Scavenging of 231Pa and thorium isotopes based on dissolved and size-fractionated particulate distributions at Drake Passage (ANTXXIV-3). *Deep Res. Part II Top. Stud. Oceanogr.* 58, 2767–2784. doi: 10.1016/j.dsr2.2010.10.040
- Walter, H. J., Rutgers van der Loeff, M. M., Höltzen, H., and Bathmann, U. (2000). Reduced scavenging of 230Th in the Weddell Sea: implications for paleoceanographic reconstructions in the South Atlantic. *Deep Sea Res. Part I Oceanogr. Res. Pap.* 47, 1369–1387. doi: 10.1016/S0967-0637(99)00094-1
- Wefer, G., Fischer, G., Fütterer, D., and Gersonde, R. (1988). Seasonal particle flux in the Bransfield Strait, Antarctica. *Deep Sea Res. Part A Oceanogr. Res. Pap.* 35, 891–898. doi: 10.1016/0198-0149(88)90066-0
- Zhang, Y., Lacan, F., and Jeandel, C. (2008). Dissolved rare earth elements tracing lithogenic inputs over the Kerguelen Plateau (Southern Ocean). *Deep Sea Res. Part II Top. Stud. Oceanogr.* 55, 638–652. doi: 10.1016/j.dsr2.2007.12.029
- Zhou, M., Zhu, Y., Ovidio, F., Park, Y.-H., Durand, I., Kestenare, E., et al. (2014). Surface currents and upwelling in Kerguelen Plateau regions. *Biogeosci. Discuss* 11, 6845–6876. doi: 10.5194/bgd-11-6845-2014

**Conflict of Interest:** The authors declare that the research was conducted in the absence of any commercial or financial relationships that could be construed as a potential conflict of interest.

Copyright © 2020 Pérez-Tribouillier, Noble, Townsend, Bowie and Chase. This is an open-access article distributed under the terms of the Creative Commons Attribution License (CC BY). The use, distribution or reproduction in other forums is permitted, provided the original author(s) and the copyright owner(s) are credited and that the original publication in this journal is cited, in accordance with accepted academic practice. No use, distribution or reproduction is permitted which does not comply with these terms.